



Swansea University
Prifysgol Abertawe



Cronfa - Swansea University Open Access Repository

This is an author produced version of a paper published in:
International Journal for Numerical Methods in Biomedical Engineering

Cronfa URL for this paper:
<http://cronfa.swan.ac.uk/Record/cronfa51923>

Paper:

Carson, J., Roobottom, C., Alcock, R. & Nithiarasu, P. (2019). Computational Instantaneous WaveFree Ratio (IFR) For PatientSpecific Coronary Artery Stenoses Using 1D Network Models. *International Journal for Numerical Methods in Biomedical Engineering*
<http://dx.doi.org/10.1002/cnm.3255>

This item is brought to you by Swansea University. Any person downloading material is agreeing to abide by the terms of the repository licence. Copies of full text items may be used or reproduced in any format or medium, without prior permission for personal research or study, educational or non-commercial purposes only. The copyright for any work remains with the original author unless otherwise specified. The full-text must not be sold in any format or medium without the formal permission of the copyright holder.

Permission for multiple reproductions should be obtained from the original author.

Authors are personally responsible for adhering to copyright and publisher restrictions when uploading content to the repository.

<http://www.swansea.ac.uk/library/researchsupport/ris-support/>

ARTICLE TYPE

Computational Instantaneous Wave-Free Ratio (iFR) For Patient-Specific Coronary Artery Stenoses Using 1D Network Models

Jason Carson^{1,2} | Carl Roobottom³ | Robin Alcock³ | *Perumal Nithiarasu¹

¹Zienkiewicz Centre for Computational Engineering, College of Engineering, Swansea University, Swansea, UK

²Data Science Building, Swansea University Mathematics School, Swansea University, Swansea, UK

³Derriford Hospital and Peninsula Medical School, Plymouth Hospitals NHS Trust, Plymouth, UK

Correspondence

*Perumal Nithiarasu, Zienkiewicz Centre for Computational Engineering, Engineering Central, College of Engineering, Swansea University Bay Campus, Swansea, SA1 8EN, UK. Email: p.nithiarasu@swansea.ac.uk

Summary

In this work we estimate the diagnostic threshold of the instantaneous wave-free ratio (iFR) through the use of a one-dimensional haemodynamic framework. To this end we first compared the computed fractional flow reserve (FFR) predicted from a 1D computational framework with invasive clinical measurements. The framework shows excellent promise and utilises minimal patient data from a cohort of 52 patients with a total of 66 stenoses. The diagnostic accuracy of the cFFR model was 75.76%, with a sensitivity of 71.43%, a specificity of 77.78%, a positive predictive value of 60%, and a negative predictive value of 85.37%. The validated model was then used to estimate the diagnostic threshold of iFR. The model determined a quadratic relationship between cFFR and the ciFR. The iFR diagnostic threshold was determined to be 0.8910 from a receiver operating characteristic curve which is in the range of 0.89-0.9 that is normally reported in clinical studies.

KEYWORDS:

haemodynamic modelling, coronary arteries, FFR, iFR

1 | INTRODUCTION

Coronary heart disease (CHD) is the leading cause of mortality worldwide and has been attributed to approximately 15.5% of deaths-per-year. The prevalence of CHD creates a significant economic burden due to the direct healthcare costs, reduced productivity, and informal public after-care caused by CHD and other cardiovascular diseases (CVD)^{1,2}. The risk factors of CHD and other types of CVD have been extensively studied and indicate the risk of developing a CVD is increased for individuals that smoke, and those who are overweight³. There have been efforts from healthcare systems aimed at encouraging populations to lead a healthier lifestyle⁴ as this has been shown to be effective at preventing many types of CVD and other diseases. However, even with this guidance the prevalence of CHD (and other types of CVD) has continued to either remain constant or increase, with a striking finding that approximately 48% of all Americans have a cardiovascular disease⁵. Due to advances in medicine with improved diagnostic and treatment tools, the mortality rates caused by CHD are reducing in high-income countries, however this is not the case in middle income and low-income countries where the number of deaths are increasing^{6,7}. The economic burden is also expected to significantly increase as health projections have indicated there will be an increase in CHD and other types of CVD in part caused by ageing populations^{8,9}. Thus it is important to not only improve access to medical facilities that includes early diagnostic and treatment methods, but to reduce the costs and increase the efficiency of the various patient treatments.

Number in the Biomedical Engineering archive: doi:10.1002/cnm.3255

CHD is caused by a narrowing (stenosis) of a coronary artery and is often from the process of atherosclerosis. The current gold standard of care for assessing the functional significance of a stenotic lesion is fractional flow reserve (FFR)^{11,12,13}. An FFR-guided treatment strategy has been shown to reduce unnecessary stenting, reduce costs, and increase patient outcomes^{14,15,16,17} compared to a strategy that utilises only quantitative coronary angiography. FFR is an invasive procedure that is performed during coronary angiography. The procedure requires a catheter and guide wire to be inserted into either the femoral artery or radial artery. The catheter is then guided to the ascending aorta where the coronary arteries are located and a pressure-sensitive wire is then used to measure the pressure ratio from a point distal of the stenosis to a point proximal to the stenosis (aorta). Critical to the technique of FFR is that the measurement is performed under hyperaemic conditions and so requires a hyperaemic-inducing drug to be administered to the patient. Hyperaemia increases the heart rate and cardiac output of the patient which increases blood flow through the coronary arteries significantly^{18,19}. However a study showed that 28% of patients experience adverse reactions to adenosine, with 8% having such a severe reaction that the adenosine infusion had to be discontinued during the procedure²⁰. Other serious reactions to adenosine have also been reported, such as bronchospasms²¹, tachyarrhythmia and cardiac arrest²², although adverse effects as serious as these are rare.

Alternative diagnostic tools for CHD are continually being developed. One such technique is diastolic FFR (dFFR)²³ which refers to a collection of variants to FFR. In the same way as the conventional measurement, dFFR requires a hyperaemic drug to be administered and the main idea behind this variant is that the largest flow rates and lowest resistances in the coronary arteries are observed during diastole. The following are the main variants of dFFR: full-diastolic FFR, where the mean FFR over the entire diastolic phase is used; mid-diastolic FFR, where the FFR is measured at a single point in time (the middle of diastole); and end-diastolic FFR, where the FFR measurement is recorded only at end-diastole by utilising an electrocardiography gating technique. End-diastolic FFR appears to be the most promising of these and has been shown to have a better correlation than conventional FFR to the FFR measured using flow-probes²⁴ although few studies on dFFR currently exist.

Another promising alternative to FFR is the instantaneous wave-free ratio (iFR)^{25,26}. The iFR procedure also requires a pressure sensitive catheter to be inserted in order to measure the pressure drop across stenotic lesion, but iFR is performed under resting conditions so does not require a hyperaemic-inducing drug to be administered. The use of iFR was initially met with significant resistance, particularly by the community who strongly supported the use of conventional FFR^{27,28} under maximum hyperemia, but many studies have shown the viability and potential of iFR in diagnosing functionally significant stenotic lesions, showing similar diagnostic accuracy to conventional FFR^{29,30,31,32,33,34,35,36,37}, and even showing a better repeatability than conventional FFR³⁸ and a stronger correlation with the coronary velocity flow reserve³⁰. Questions still remain on whether iFR can reliably be used to replace FFR as several studies have shown mismatches in patient categorisation between iFR and the clinically trusted technique of conventional FFR³², while the reasons for these disagreements were not fully understood. However, it has since been shown that the differences between the two indices was more likely related to FFR overestimating the severity of the stenosis, rather than iFR underestimating the severity³⁹. A hybrid iFR-FFR approach has also been proposed^{40,38} that enhances the diagnostic accuracy while reducing the number of patients who require adenosine to be administered. In the SYNERGY-FLAIR study⁴¹ iFR was shown to have non-inferior patient outcomes when compared with conventional FFR, and is considered a practical alternative to FFR that can avoid adverse patient reactions to hyperaemic drugs while costing less. The standard cut-off points of FFR and iFR are generally 0.8 and 0.89 respectively, although different cut-off points have been proposed for iFR, ranging from 0.83 to 0.92^{29,42,36}, implying that the true cut-off point for iFR is still uncertain. In the FFR-iFR hybrid approach a lesion with an iFR value in the grey-zone of 0.86-0.93 also undergoes FFR, while an iFR value of less than 0.86 requires treatment, and lesions with iFR values above 0.93 do not undergo surgical treatment^{40,38}.

Non-invasive methods for estimating FFR are based on reconstructed and segmented coronary computed tomography angiography (CCTA) images. Techniques from computational fluid dynamics are then applied to the patient geometry to determine the FFR while avoiding the need for any invasive cardiac catheterisation. The technique is often called computed FFR (cFFR), and relies on the estimation of several important modelling components that includes the patients' cardiovascular response to the hyperaemic drug infusion, that influences the elasticity of arteries, and boundary conditions of the model. Different computational methodologies have been proposed which include computationally expensive three-dimensional models^{43,44,45,46,47,48,49,50}, and reduced-order models^{51,52,53,54,55,56,57,58,59,60}. One dimensional-models have been shown to have excellent agreement with three-dimensional models^{53,60} but can be computed in seconds, rather than hours (for 3D). Computational models of iFR have been proposed but are generally compared with: only invasive FFR measurements⁶¹, in which the estimated iFR cut-off point was 0.82, however, rigid-wall conditions were assumed which is known to significantly overestimate the pressure drop across a stenosis for cFFR⁶² and is likely to have a similar impact for ciFR; or utilised in a hybrid-approach⁶³, although a monte-carlo simulation that utilises a lumped model⁶⁴ without patient-specific geometry has been implemented. Nevertheless, a comparison

Stenosis Location ($n = 66$)	n (%)
LCA	3 (4.5)
LAD	40 (60.6)
LCX	7 (10.6)
DA	3 (4.5)
MA	2 (3.0)
IA	1 (1.5)
RCA	10 (15.2)

FFR Characteristics ($n = 66$)	n (%)
FFR < 0.8	21 (31.8)
FFR \geq 0.8	45 (68.2)

TABLE 1 Distribution of stenosis location among the cohort and characteristics of the FFR measurements.

When the invasive iFR measurement and computational iFR was performed in⁶⁵. However, the computational methodology is not described in⁶⁵, requires images from invasive coronary angiography, and the cut-off point for iFR is assumed to be 0.89.

The purpose of this work is to compare clinical FFR measurements with cFFR estimated via a one-dimensional haemodynamic model in order to validate the cFFR strategy, and to determine the diagnostic cut-off point of iFR through the application of computational models on patient-specific coronary arterial networks that have been extracted from non-invasive CCTA. By using the same extracted patient-specific coronary network geometry, the boundary conditions of the 1D model can be easily adjusted to change from hyperaemic conditions to resting physiological conditions, which essentially adapts the cFFR model into a ciFR model. The correlation between ciFR and cFFR, and the clinically accepted FFR diagnostic threshold of 0.8 will then be used in order to estimate the diagnostic threshold for the iFR procedure. An advantage of using this computational framework is that variability of surgical techniques and of the patients' physiological conditions can be eliminated which allows the iFR diagnostic threshold to be estimated in a more controlled environment. The patient data was collected retrospectively and no patient specific measurements were used to aid the model parameter estimation.

The paper is organised into the following parts: in section 2 the characteristics of the data utilised in this paper and the one-dimensional computational framework are described; the results in section 3 begin by comparing the cFFR predicted by the computational framework with the clinically invasive FFR measurements, this leads on to the comparison of the model predicted FFR and iFR values; in section 4 the results are discussed and compared with previous findings in literature; and finally the main conclusions of the work are presented in section 5.

2 | MATERIALS AND METHODS

2.1 | Study characteristics

In this study an anonymised retrospective data set of 52 patients with a total of 66 lesions was collected. The exact clinical FFR values were not available for a subset of 10 of these patients (15 stenosis). Only whether the FFR was positive or negative for these patients was available. An overview of the locations and characteristics of these stenotic lesions can be seen in table 1. The majority of lesions (78.43%) considered in this work are in the intermediate FFR range of $0.7 < FFR < 0.9$, with 68.2% of the total lesions having a negative FFR value and 31.8% having a positive FFR value. A stenosis location of the left anterior descending artery (LAD) was most prevalent (60.6%). Patients who had undergone previous coronary surgical interventions were included only if the intervention was performed within vessels that were not of interest for this study. Patients with serial stenoses and CCTA data images which contained motion artefacts and significant levels of calcification were also included in this study. Table 2 shows statistics on the characteristics of the CCTA images, that includes information on the percentage of lesions with calcification and motion artefacts that are present.

Stenosis no. and type	Single focal	Single diffuse	Multiple
	50	16.67	33.33
Stent no.	0	1	2
	87.88	10.61	1.52
Occlusion no.	0	1	2
	83.33	15.15	1.52
Bifurcation	no	within 1-2mm	within 1mm
	50	30	20
Calcification	none	minor	major
	22.73	48.48	28.79
Motion artefacts	none	minor	major
	74.24	19.7	6.06

TABLE 2 CCTA and stenosis characteristics. Percentage of cases that includes: single focal stenosis, single diffuse stenosis, or multiple stenoses (either focal or diffuse); number of stents and vessel occlusions; number of cases with a stenosis near (between 2mm and 5mm), and at (within 2mm) of a bifurcation; whether calcification is present, and to what severity (minor is less likely to affect segmentation accuracy, while major is likely to impact segmentation accuracy); and whether motion artefacts are present and to what severity. All values given as a percentage of the cohort

2.2 | Computed FFR methodology

The segmentation of CCTA images, centreline and vessel geometry extraction, were all performed in the image segmentation software VMTKLab, (Orobix, Italy).

2.2.1 | One-dimensional haemodynamic model

The modelling methodology implemented in this work is described in⁶⁶ and involves the one-dimensional haemodynamic equations in a pressure-volumetric flow rate formulation^{67,66} that is given by: the conservation of mass

$$C_a \frac{\partial P}{\partial t} + \frac{\partial Q}{\partial x} = 0, \quad (1)$$

where C_a is the vessel compliance, P is the mean hydrostatic pressure in a cross section, and Q is the volumetric flow rate; and the momentum equation

$$\frac{\rho}{A} \frac{\partial Q}{\partial t} + \frac{\rho}{A} \frac{\partial \left(\frac{Q^2}{A} \right)}{\partial x} + \frac{\partial P}{\partial x} = \frac{22\mu\pi Q}{A^2}, \quad (2)$$

where $\rho = 1.05\text{g/cm}^3$ is the density of blood, A is the cross-sectional area of the vessel, $\mu = 0.04\text{Poise}$ is the blood viscosity, and the magnitude of the viscous coefficient of 22 is from⁶⁸ and was shown to be the best fit to experimental data for the coronary system. The vessel compliance is calculated as $\frac{\partial A}{\partial P}$ from the following visco-elastic constitutive law⁶⁹,

$$P - P_0 - P_{ext} = \frac{2\rho c_0^2}{b} \left(\left(\frac{A}{A_0} \right)^{b/2} - 1 \right) + \frac{\Gamma}{A_0 \sqrt{A}} \frac{\partial A}{\partial P} \frac{\partial P}{\partial t}, \quad (3)$$

with

$$b = \frac{2\rho c_0^2}{P_0 - P_{collapse}} \quad (4)$$

where the reference wave speed c_0 is calculated from the vessel diameter using the empirical formula^{70,69} as

$$\frac{2}{3\rho} [k_1 \exp(k_2 D_0/2) + k_3], \quad (5)$$

where D_0 is the reference diameter, and the fitting parameters are $k_1 = 20\text{ g/s}^2/\text{cm}$, $k_2 = -22.5\text{ cm}^{-1}$, and $k_3 = 86.5\text{ g/s}^2/\text{cm}$. The reference pressure P_0 is set to equal the diastolic pressure, and the collapsing pressure $P_{collapse} = -10\text{ mmHg}$. The wall

viscous coefficient Γ^{69} is calculated from

$$\Gamma = \frac{100}{D} + 400, \quad (6)$$

where D is the vessel lumen diameter.

The system of equations are solved using a sub-domain collocation scheme^{71,66} that is second-order accurate in both time and space.

2.2.2 | Boundary conditions

The inlet and outlet boundary conditions for the model are predicted by using a two-tiered parameter estimation technique. The first tier utilises a general, non-patient-specific, closed-loop 1D-0D network to estimate the volumetric inflow rate for the coronary arteries; while the second tier uses the inflow rate determined from the first tier as the coronary inflow boundary condition, and then estimates the vascular bed resistances for the patient-specific coronary arterial network that was extracted from the CCTA image data.

First-tier of the parameter estimation

The first-tier of the parameter estimation utilising the closed-loop cardiovascular model with an initial and adaptive parameter estimation technique that are described in^{66,72}. The purpose of this technique is to provide an estimate for the volumetric flow rate at the inlet of the coronary arteries, and to provide an estimate for the left and right ventricular pressures, as they add an external pressure to the coronary vascular beds. The first tier is performed twice: once for hyperaemic conditions, and once for resting conditions. As no clinical data on patient pressures or heart rates were available, only population averaged values from literature were used. The population averaged values for both hyperaemic and resting conditions (assumed the same for all patients) are described in table 3, and are from population averages of previous coronary artery studies^{18,19}. The assumption that the values of parameters such as the heart rate and blood pressures are consistent among patients is valid as: FFR has been shown to be independent of heart rate, blood pressure and heart contractility^{73,12}, the relationship between iFR and FFR is also independent of heart rate²⁶, and iFR has also been shown to be independent of heart rate, blood pressure and heart contractility²⁵.

An additional change from the resting condition to the hyperaemic condition is performed by reducing the total coronary vascular bed resistance by 78 %, this causes the mean flow rate in the coronary arteries for the hyperaemic condition to be 3.5 times larger than in resting conditions¹⁸. This means that there are only two different defined inflow waveforms for the coronary arteries, which allows a more straightforward comparison between cFFR and ciFR.

Second-tier of the parameter estimation

The inlet boundary condition for all simulations is a defined flow rate (one for hyperaemic conditions, and one for resting conditions) that was generated by the closed-loop cardiovascular model described in the first parameter estimation tier. The second tier uses the patient-specific coronary geometry that was extracted via segmentation. The outlet boundary condition is a lumped-parameter model that includes external pressure from the left and right ventricles⁶⁶ (saved from the first-tier of the parameter estimation). The total coronary resistance of each branch is calculated using the commonly used relation

$$R_i = \frac{\frac{1}{3}\text{Systolic Pressure} + \frac{2}{3}\text{Diastolic Pressure}}{Q_i}, \quad (7)$$

where the subscript i represents the branch (left or right) of the coronary artery network, and Q_i is the defined inflow into the coronary branch from the first tier. The resistance of each branch is then distributed to each terminal vessel using the proximal Murray's law with a power of 2.27⁷⁴. This means that the second tier of parameter identification relies solely on the patient specific geometry for the distribution of the vascular resistance.

Model cFFR and ciFR

Both conventional FFR and iFR are measurements that involve the ratio of the pressure proximal (P_p) to a stenosis (usually aortic pressure), and the pressure distal (P_d) to a stenosis. The ratio of P_d/P_p is used for all cases. The main differences between the two methods are as follows: Conventional FFR is measured under maximal hyperaemic conditions, which requires a drug such as adenosine to be administered and is the mean of the pressure ratio P_d/P_p over one cardiac cycle (in clinical practice multiple cycles); iFR is performed under resting conditions and is the mean of the pressure ratio P_d/P_p during the wave-free period, which is shown in Figure 1 as the grey shaded region. In this model ciFR is assumed to begin $1/5^{th}$ into diastole to the end of the cardiac cycle.

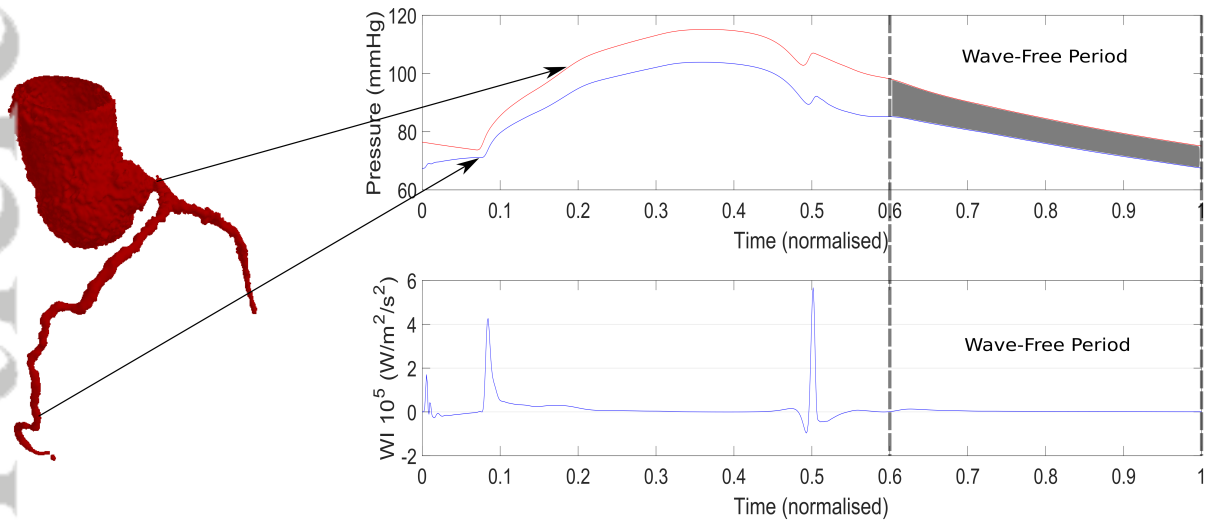


FIGURE 1 Overview of iFR (average P_d/P_p of the shaded region) and example of the wave-free period during diastole

	resting	hyperaemic
systolic pressure (mmHg)	115	115
diastolic pressure (mmHg)	74	70
cardiac output (L/min)	5.19	7.6
heart rate (BPM)	65	90

TABLE 3 Parameters used in the model for resting and hyperaemic conditions

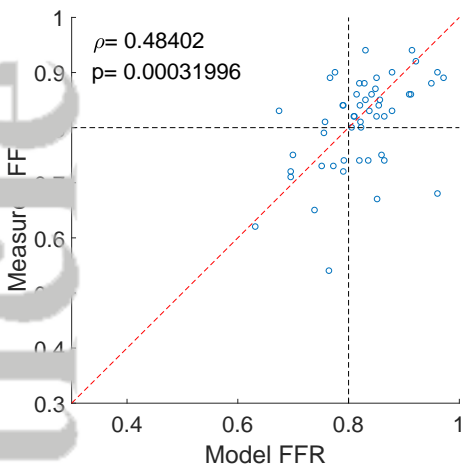
no. true positive	15
no. false positive	10
no. true negative	35
no. false negative	6
Sensitivity, %	71.43
Specificity, %	77.78
PPV, %	60.00
NPV, %	85.37
Diagnostic accuracy %	75.76

TABLE 4 Diagnostic results of cFFR prediction showing the total number of true positive, false positive, true negative, false negative, sensitivity, specificity, positive predictive value, negative predictive value, and diagnostic accuracy

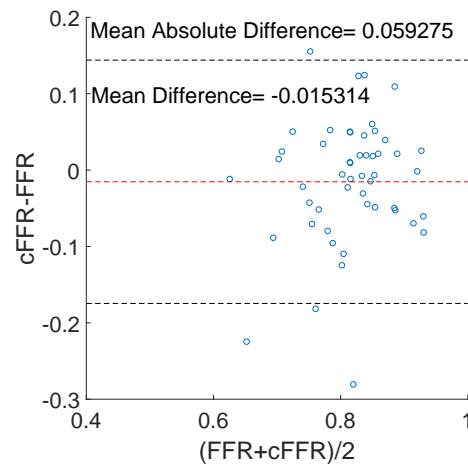
3 RESULTS

3.1 cFFR comparison with clinical invasive FFR

An overview of results for the reduced-order cFFR model in comparison with the invasive clinical FFR measurement is shown in table 4 with the correlation and Bland-Altman graphs shown in figure 2. The diagnostic accuracy of the model is 75.76%. The mean absolute difference between the cFFR and FFR values is 0.059, with a mean difference of -0.015 and a standard deviation of 0.0813. A Pearson coefficient of 0.484 shows a moderate linear correlation between the cFFR and invasive FFR values.



(a) FFR against cFFR, with Pearson correlation ρ and p -value with a line of equality (red line)



(b) Bland-Altman of FFR and cFFR with the mean difference in values given by the red line and the black line representing the 95% confidence interval

FIGURE 2 Comparison cFFR with the invasive FFR measurements

3.2 Correlation between cFFR and ciFR

The main results are shown in figure 3 with a Pearson correlation coefficient of $\rho = 0.95352$ showing a strong linear correlation between cFFR and ciFR values. The Bland-Altman plot shown in figure 3b shows the mean difference between cFFR and ciFR is 0.08402.

Lines of best-fit can be used to aid determining the correct relationship between cFFR and ciFR, as many correlation measures are based on the assumption of a linear relation. Figure 3a compares ciFR to cFFR using the following polynomials of best-fit: the linear polynomial

$$\text{ciFR}_1 = 0.6469\text{cFFR} + 0.3688, \quad (8)$$

the quadratic polynomial

$$\text{ciFR}_2 = -0.5926\text{cFFR}^2 + 1.5616\text{cFFR} + 0.0218, \quad (9)$$

and the cubic polynomial

$$\text{ciFR}_3 = 0.6770\text{cFFR}^3 - 2.1472\text{cFFR}^2 + 2.7307\text{cFFR} - 0.2654. \quad (10)$$

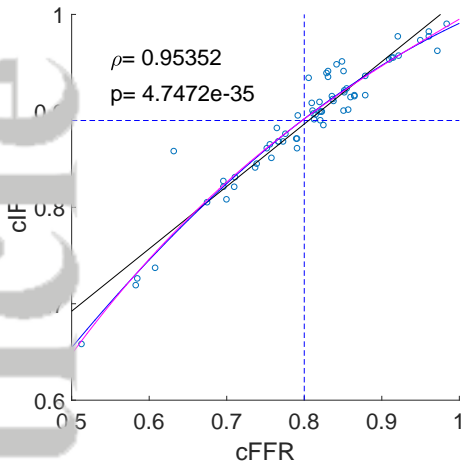
The polynomials of best fit allow the determination of the cut-off point for iFR by comparing the iFR value to the diagnostic cut-off point of FFR = 0.8. The linear polynomial estimates a value of $\text{ciFR}_1 = 0.8863$, the quadratic polynomial estimates $\text{ciFR}_2 = 0.8918$, and the cubic polynomial estimates $\text{ciFR}_3 = 0.8916$. The results indicate that the relationship between FFR and iFR is better described by a second-order polynomial that provides an excellent fit for the data.

Receiver operating characteristic curve

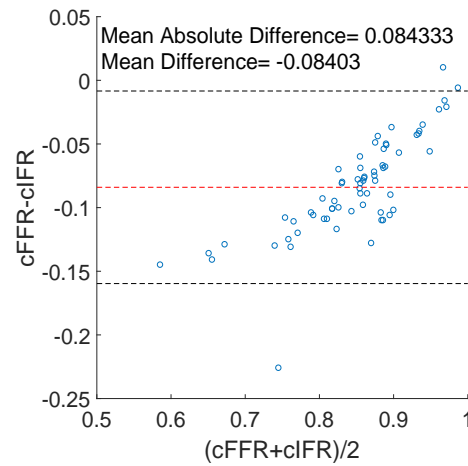
It is common to use receiver operating characteristic curves (ROC) to determine the optimum threshold of a methodology. Figure 4 shows the ROC curve of ciFR for different threshold values, when compared with cFFR (with a threshold of 0.8), where the area under the curve is AUC= 0.9971. The optimum threshold for ciFR via ROC analysis is determined to be ciFR= 0.8910.

DISCUSSION

The performance of the reduced-order cFFR methodology in comparison with the invasive FFR measurements is very satisfactory at this early stage of development and shows a similar level of accuracy to several three dimensional cFFR methodologies⁷⁵. The diagnostic accuracy of the reduced-order methodology is 75.76% which is in the region seen from other studies, however the current methodology did not have patient information along with the CCTA data, and hence a population average blood pressure, heart rate, and cardiac output from published studies^{18,19} was chosen. The utilisation of routinely measured patient

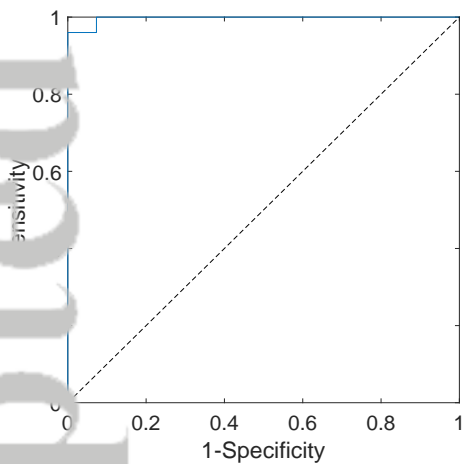


(a) ciFR against cFFR, with Pearson correlation ρ and p -value. The lines of best-fit are a linear (black line), quadratic (blue line), and cubic (purple line). The horizontal and vertical dashed blue lines are the iFR and FFR cut-off points, assumed to be 0.89 and 0.8 respectively

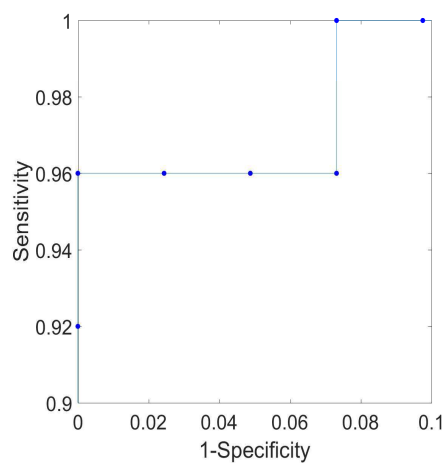


(b) Bland-Altman of ciFR and cFFR with the mean difference in values given by the red line and the black line representing the 95% confidence interval

FIGURE 3 Comparison of the model predicted cFFR and ciFR values



(a) Full threshold range for ciFR



(b) reduced threshold range for ciFR

FIGURE 4 Receiver operating characteristic curve of cFFR and ciFR over the a range of threshold points for ciFR

data may improve the models estimation of cFFR by integrating more patient-specific parameters. Even with the lack of patient-specific data the strategy performed well with a sensitivity of 71.43%, a specificity of 77.78%, a positive predictive value of 60% and a negative predictive value of 85.37%. Furthermore, the mean difference between cFFR and invasive FFR was -0.015314 , which is lower in magnitude than the mean difference shown in the three dimensional methodology performed for different patient data in the DISCOVER-FLOW⁴³ (0.022), DeFACTO⁴⁴ (0.058) and NXT⁴⁵ (0.03) studies. The standard deviation of the reduced-order model is 0.0813, which is close to the lowest standard deviation from the other studies of 0.074⁴⁵. The model predicted cFFR showed a lower Pearson correlation with the FFR than in other studies⁷⁵, however this could be attributed to the smaller cohort size and the low range of measured FFR values, as the majority (78.43%) of invasive cFFR measurements were in the range $0.7 < \text{FFR} < 0.9$. Overall the results indicate that the reduced-order methodology presented here provides a high level of diagnostic accuracy for cFFR.

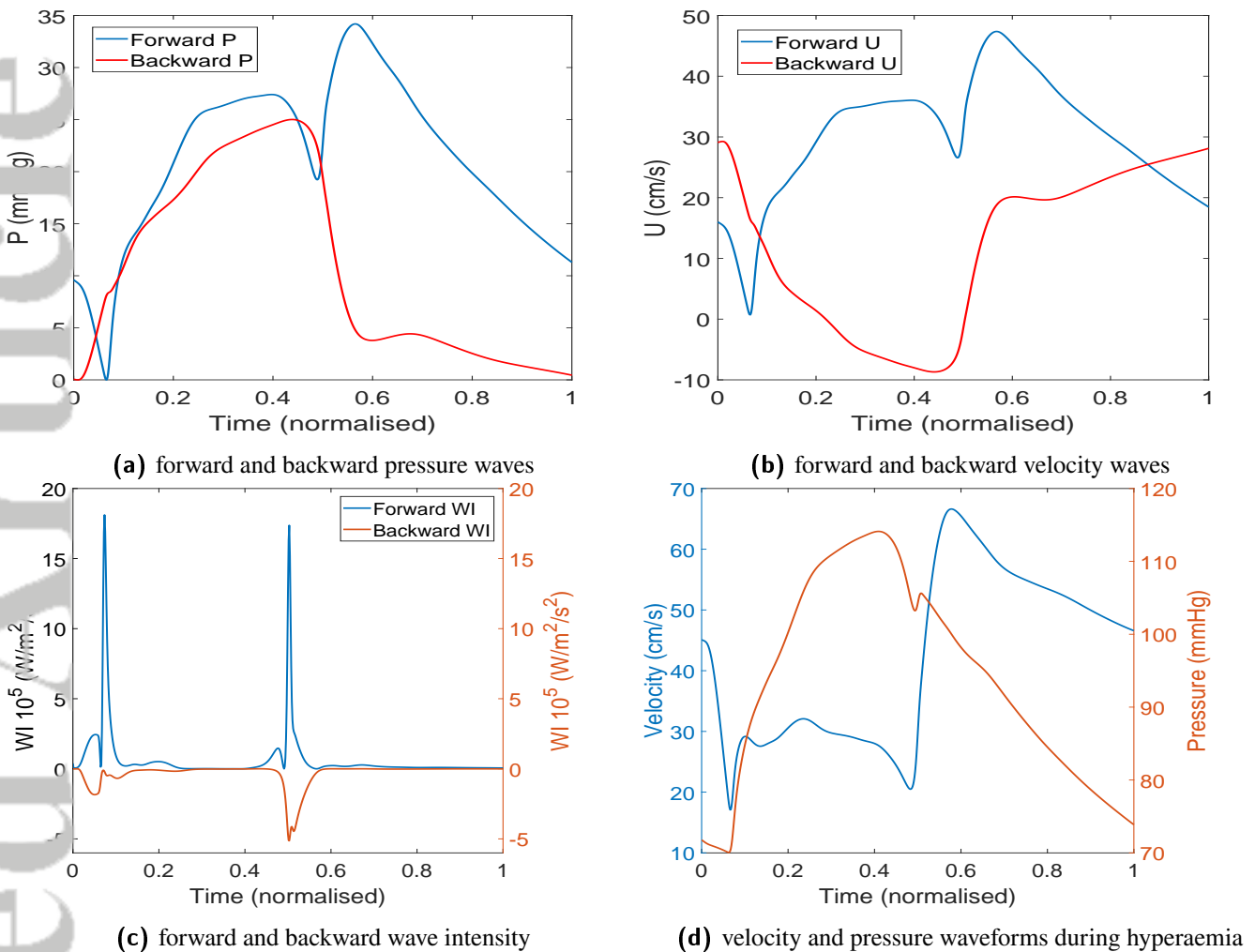


FIGURE 5 Separation of forward and backward-propagating waves in the left main coronary artery

The framework presented does need to be tested on a larger cohort in fully blinded conditions and ideally using prospective data. In the current cohort there are several patients that would have been excluded in other studies due to poor image quality⁷⁵, therefore the diagnostic performance of the methodology was not the only objective of this paper. The main reason for the comparison at this stage was to validate the methodology and provide confidence that the predicted cFFR values of the model are close to the invasive FFR measurements, which in turn will provide an indication that the iFR values predicted by this model can be trusted. The methodology also allows the computed iFR values to be implemented within the same framework as cFFR and thus the developed software could easily be adapted to automatically perform the hybrid iFR-FFR technique^{40,38}. The use of the same inlet volumetric flow rate and estimated heart rate also ensures that only the geometry and downstream resistance of the coronary network are the main variables which affect the FFR and iFR value predictions.

4.1 cFFR and ciFR comparison

The use of iFR in combination with, or instead of FFR has received increased attention in recent years. However many studies use different threshold values of iFR to determine whether a patient needs further treatment³⁶. The estimation of the iFR diagnostic threshold ranges from 0.92⁷⁶, 0.9^{31,29,77,78}, 0.89^{79,80}, 0.88⁸¹, and even 0.83⁸², which obviously indicates that the best diagnostic threshold for iFR is still not known. The results from this paper indicate that the diagnostic threshold for iFR is close to 0.89, and that the relationship between ciFR and cFFR is quadratic in nature. This agrees with the observed behaviour from a comparison of invasive FFR and iFR measurements³⁹. Other studies have reported an approximately linear behaviour from measurements^{32,83}, and from a monte-carlo simulation with a lumped parameter model⁶⁴, however there is a noticeable deviation from the linear

line of best fit at lower FFR and iFR values, which indicates that a non-linear relationship would provide a better fit between FFR and iFR measures.

Another interesting aspect to consider is whether the cardiovascular system is a pressure-driven or flow-driven system, which depends on whether the heart is a flow generator or pressure generator⁸⁴. The fact that the heart contracts and creates a pressure that acts on coronary capillary vessels complicates matters as there would be: a forward-propagating pressure wave originating from the heart that travels into the aorta and then through the coronary arteries from the proximal to distal location; and also a backward-propagating pressure wave that originates from the coronary capillaries as a result of the contracting heart that travels from the distal region of the coronary arteries to the proximal region⁸⁵. In reality it is more likely that the cardiovascular system is a complex combination of both pressure-driven and flow-driven phenomena⁸⁴. However, due to the forward and backward pressure waves during systole and at the start of diastole, which can be seen in figure 5, a pressure index based on the diastolic pressure could be more reliable as the lowest resistance to flow in the coronary arterial network is observed during diastole.

Many of the fundamental assumptions needed for FFR have since been proven incorrect. For example, the pressure and flow were assumed to be directly proportional (have a linear relationship) when the resistance is constant and minimal⁸⁶ but has since been shown have a curvilinear relationship experimentally⁸⁷ and mathematically. This essentially means that FFR relies on the assumption that the characteristics of flow are the same in both diseased and healthy vessels. The assumption of the micro-circulatory resistance being constant and minimal during hyperaemia is also questionable and has been proven incorrect in the presence of several conditions including micro-vascular dysfunction⁸⁶. In hyperaemia the resistance averaged over a cardiac period may be consistent during hyperaemia, but the micro-vascular resistance will vary significantly over a cardiac cycle as the heart contraction squeezes on the micro-circulation during systole which increases resistance⁸⁸. These assumptions are not required for iFR, instead the main assumption for iFR is that the resistance of the micro-circulation is stable during the wave-free period, which is during a period in diastole where no waves are generated, such as seen in figure 5c from a normalised time of 0.6 to 1.

Many studies compare the diagnostic performance of iFR to FFR and consider the latter index to be the 'perfect measure'. This generally means that iFR looks worse than FFR, but this is a rather unfair comparison. Further studies have indicated that iFR and FFR have a similar number of negative cardiovascular events after one year⁴¹ and thus is at least on-par with FFR. Several studies have compared iFR and FFR^{29,30,31,32,33,34,35,36,37}, however only one attempted to explain the cause of the various diagnostic disagreements observed between iFR and FFR³⁹. The study concluded that it was actually the FFR that was likely overestimating the severity of the stenosis due to the hyperaemic condition rather than iFR underestimating the stenosis, and for the cases that had a positive FFR but negative iFR the observed coronary flow characteristics were similar to that seen in angiographically unobstructed vessels, which indicates that iFR may be the more reliable and suitable measure.

From a non-invasive standpoint for the determination of iFR and FFR, iFR has more advantages over FFR as it does not require determination of how the patient will react to the administered hyperaemic inducing drug. Many cardiac and haemodynamic parameters can be measured by non-invasive means, including cardiac output estimations, brachial artery blood pressures, and heart rate. These parameters can be directly utilised by any non-invasive iFR model predictions rather than attempting to predict the effects of a hyperaemic condition which are variable between patients and are required for FFR estimations. In addition, the majority of the patient CCTA scans are performed at resting conditions. This is particularly important as the inducing of hyperaemic conditions through the use of a drug, such as adenosine, was observed to increase coronary vessel diameters by up to 15%⁸⁹, thus there is even significant uncertainty for cFFR regarding the actual patient geometry that is extracted from CCTA

4.2 Limitations

The main limitations of this study are that the size of the cohort is relatively small with 52 patients and a total of 66 stenoses. Furthermore, we assume that there are no pressure losses at vessel junctions, and do not have patient data such as age, blood pressures, heart rate, or gender, which may play a role in FFR prediction. We do not have any invasive iFR measurements, only FFR measurements and the patient CCTA images were available. As the data is retrospective, we do not know the exact location of the pressure measurement taken during invasive FFR, as only the general location is normally recorded in the clinic. However, the main target of this study was to determine the diagnostic threshold of iFR in a more controlled environment, and although the cFFR performance of the model is very good, it was not the focus of this paper and thus the additional patient data is not of importance here.

It has been observed that vessels with coronary artery disease⁹⁰ can cause a long-term auto-regulatory response in the coronary micro-vasculature resistance to preserve flow. This may impact the accuracy of the flow estimates. However, it is not known how or if this auto-regulation affects flow rates in hyperaemia; and would add an additional unknown and source of uncertainty in the model, which will make comparison between FFR and iFR more challenging. Thus we have not included this auto-regulatory response in this study.

5 | CONCLUSIONS

The diagnostic performance of the cFFR with the invasive FFR measurement is very promising. The methodology showed a strong correlation between cFFR and FFR than in other studies, but also showed the lowest magnitude of mean difference and one of the lowest standard deviations between the computed and measured FFR when compared to other studies. The lower correlation coefficient may be due to the lower patient numbers considered in this cohort and also on the non-selective nature in this study with regards to image quality such as the presence of significant motion artefacts, blooming artefacts, and high levels of calcification that can have a large impact on the accuracy of the segmentation process. The methodology must now be validated on a significantly larger cohort in a fully blinded fashion and ideally prospectively in order to improve the confidence in the 1D modelling methodology for both FFR and iFR predictions.

A comparison between cFFR and computed iFR was also performed by utilising the patient CCTA data. The model predicted an iFR diagnostic cut-off point of 0.891 with the correlation and polynomial of best fit between cFFR and ciFR being quadratic in nature. Further studies involving comparisons between FFR and iFR must be performed in order to determine whether FFR or iFR is the more reliable measure. There is a significant advantage of iFR, as it does not require a hyperaemic drug infusion which can cause negative side effects in patients and would also be less expensive. When considering a computational methodology for prediction purposes, ciFR is also more attractive as a diagnosis index when compared to cFFR, as the patients non-invasive measurements can be utilised directly without the need to predict hyperaemic conditions.

ACKNOWLEDGEMENTS

The authors gratefully acknowledge financial support from UKRI and MRC under the grant MR/S004076/1.

References

1. World Health Organization WH. *Global Atlas on Cardiovascular Disease Prevention and Control*. WORLD HEALTH ORGN . 2012.
2. Benjamin EJ, Blaha MJ, Chiuve SE, et al. Heart Disease and Stroke Statistics—2017 Update: A Report From the American Heart Association. *Circulation* 2017; 135(10). doi: 10.1161/cir.0000000000000485
3. Virtanen M, Vahtera J, Singh-Manoux A, Elovainio M, Ferrie JE, Kivimäki M. Unfavorable and favorable changes in modifiable risk factors and incidence of coronary heart disease: The Whitehall II cohort study. *International Journal of Cardiology* 2018; 269: 7–12. doi: 10.1016/j.ijcard.2018.07.005
4. Gunn AL. Effectiveness of Lifestyle Physical Activity Interventions to Reduce Cardiovascular Disease. *American Journal of Lifestyle Medicine* 2009; 3(1_suppl): 11S–18S. doi: 10.1177/1559827609336067
5. Benjamin EJ, Muntner P, Alonso A, et al. Heart Disease and Stroke Statistics—2019 Update: A Report From the American Heart Association. *Circulation* 2019; 139(10). doi: 10.1161/cir.0000000000000659
6. Bengold JA, Asaria P, Francis DP. Mortality from ischaemic heart disease by country, region, and age: Statistics from World Health Organisation and United Nations. *International Journal of Cardiology* 2013; 168(2): 934–945. doi: 10.1016/j.ijcard.2012.10.046
7. Bhatnagar P, Wickramasinghe K, Wilkins E, Townsend N. Trends in the epidemiology of cardiovascular disease in the UK. *Heart* 2016; 102(24): 1945–1952. doi: 10.1136/heartjnl-2016-309573

8. Mathers CD, Loncar D. Projections of Global Mortality and Burden of Disease from 2002 to 2030. *PLoS Medicine* 2006; 3(11): e442. doi: 10.1371/journal.pmed.0030442
9. Malahur G, Badimon JJ, Bugiardini R, Badimon L. Perspectives: The burden of cardiovascular risk factors and coronary heart disease in Europe and worldwide. *European Heart Journal Supplements* 2014; 16(suppl A): A7–A11. doi: 10.1093/eurheartj/sut003
10. Roth GA, Johnson C, Abajobir A, et al. Global, Regional, and National Burden of Cardiovascular Diseases for 10 Causes, 1990 to 2015. *Journal of the American College of Cardiology* 2017; 70(1): 1–25. doi: 10.1016/j.jacc.2017.04.052
11. Pijls N, De Bruyne B, Peels K, et al. Measurement of fractional flow reserve to assess the functional severity of coronary-artery stenoses. *N. Engl. J. Med.* 1996; 334: 1703–1708.
12. Kolli KK, Banerjee RK, Peelukhana SV, et al. Influence of heart rate on fractional flow reserve, pressure drop coefficient, and lesion flow coefficient for epicardial coronary stenosis in a porcine model. *American Journal of Physiology-Heart and Circulatory Physiology* 2011; 300(1): H382–H387. doi: 10.1152/ajpheart.00412.2010
13. Botfi A, Jeremias A, Fearon W, et al. Expert consensus statement on the use of fractional flow reserve, intravascular ultrasound, and optical coherence tomography: A consensus statement of the Society of Cardiovascular Angiography and Interventions. *Catheter Cardiovasc. Interv.* 2014; 83: 509–518.
14. Pijls N, Schaardenburgh vP, Manoharan G, et al. Percutaneous coronary intervention of functionally nonsignificant stenosis: 5-year follow-up of the DEFER Study. *J. Am. Coll. Cardiol.* 2007; 49: 2105–2111.
15. Tonino P, Fearon W, De Bruyne B, et al. Angiographic versus functional severity of coronary artery stenoses in the FAME study fractional flow reserve versus angiography in multivessel evaluation. *J. Am. Coll. Cardiol.* 2010; 55: 2816–2821. doi: 10.1016/j.jacc.2009.11.096
16. Pijls N, Fearon W, Tonino P, et al. Fractional flow reserve versus angiography for guiding percutaneous coronary intervention in patients with multivessel coronary artery disease: 2-year follow-up of the FAME (Fractional Flow Reserve Versus Angiography for Multivessel Evaluation) study. *J. Am. Coll. Cardiol.* 2010; 56: 177–184. doi: 10.1016/j.jacc.2010.04.012
17. Fearon W, Bornschein B, Tonino P, et al. Economic evaluation of fractional flow reserve-guided percutaneous coronary intervention in patients with multivessel disease. *Circulation* 2010; 122: 2545–2550. doi: 10.1161/CIRCULATION-AHA.109.925396
18. Watzinger N, Lund GK, Saeed M, et al. Myocardial blood flow in patients with dilated cardiomyopathy: Quantitative assessment with velocity-encoded cine magnetic resonance imaging of the coronary sinus. *Journal of Magnetic Resonance Imaging* 2005; 21(4): 347–353. doi: 10.1002/jmri.20274
19. Wieneke H, Birgelen vC, Haude M, et al. Determinants of coronary blood flow in humans: quantification by intracoronary Doppler and ultrasound. *Journal of Applied Physiology* 2005; 98(3): 1076–1082. doi: 10.1152/jappphysiol.00724.2004
20. VoigtlÄnder T, Schmermund A, Bramlage P, et al. The Adverse Events and Hemodynamic Effects of Adenosine-Based Cardiac MRI. *Korean Journal of Radiology* 2011; 12(4): 424. doi: 10.3348/kjr.2011.12.4.424
21. Bencharz D, Quigley AM, Hall M, Wagner TLJ. Rapid and Severe Adverse Reaction to Adenosine During a Pharmacological Stress Test for a Myocardial Perfusion Scan. *Clinical Nuclear Medicine* 2013; 38(9): 758. doi: 10.1097/rlu.0b013e31829f5993
22. El-Menyar A, Gehani A. Adenosine-induced tachyarrhythmia and cardiac arrest. *Future Cardiology* 2010; 6(4): 433–436. doi: 10.2217/fca.10.66
23. Abe M, Tomiyama H, Yoshida H, Doba N. Diastolic Fractional Flow Reserve to Assess the Functional Severity of Moderate Coronary Artery Stenoses. *Circulation* 2000; 102(19): 2365–2370. doi: 10.1161/01.cir.102.19.2365
24. Chalyan DA, Zhang Z, Takarada S, Molloy S. End-Diastolic Fractional Flow Reserve. *Circulation: Cardiovascular Interventions* 2014; 7(1): 28–34. doi: 10.1161/circinterventions.113.000327

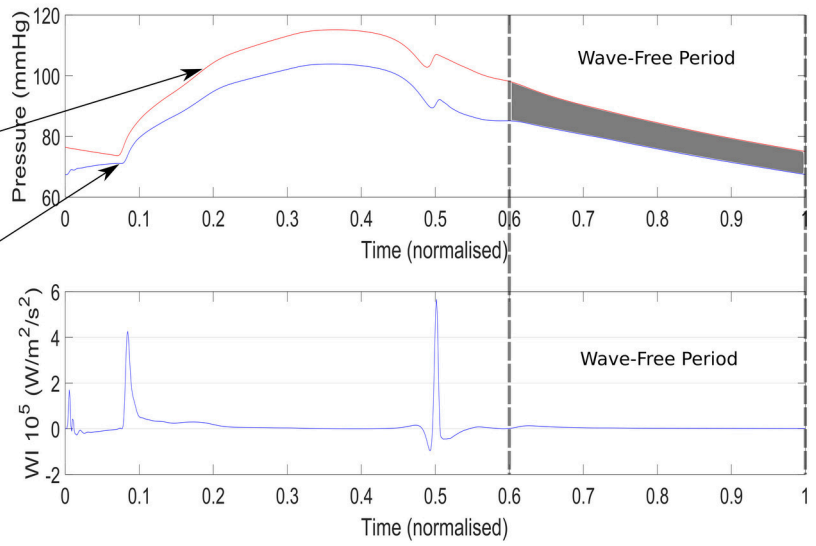
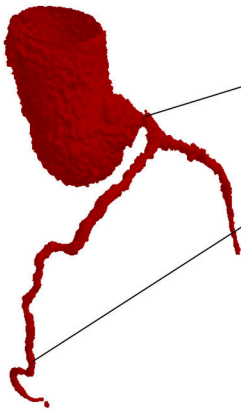
25. Sen S, Escaned J, Malik I, et al. Development and validation of a new adenosine-independent index of stenosis severity from coronary wave-intensity analysis: results of the ADVISE (ADenosine Vasodilator Independent Stenosis Evaluation) study. *J. Am. Coll. Cardiol.* 2012; 59: 1392–1402. doi: 10.1016/j.jacc.2011.11.003
26. Sen S, Asrress KN, Nijjer S, et al. Diagnostic Classification of the Instantaneous Wave-Free Ratio Is Equivalent to Fractional Flow Reserve and Is Not Improved With Adenosine Administration. *Journal of the American College of Cardiology* 2013; 61(13): 1409–1420. doi: 10.1016/j.jacc.2013.01.034
27. Fudzinski W, Waller AH, Kaluski E. Instantaneous Wave-Free Ratio and Fractional Flow Reserve: Close, But Not Close Enough!. *Journal of the American College of Cardiology* 2012; 59(21): 1915–1916. doi: 10.1016/j.jacc.2012.01.047
28. Pijls NH, Veer tMV, Oldroyd KG, et al. Instantaneous Wave-Free Ratio or Fractional Flow Reserve Without Hyperemia. *Journal of the American College of Cardiology* 2012; 59(21): 1916–1917. doi: 10.1016/j.jacc.2012.01.049
29. Jeremias A, Maehara A, Génereux P, et al. Multicenter Core Laboratory Comparison of the Instantaneous Wave-Free Ratio and Resting Pd/Pa With Fractional Flow Reserve. *Journal of the American College of Cardiology* 2014; 63(13): 1253–1261. doi: 10.1016/j.jacc.2013.09.060
30. Petraco R, Hoef v. dTP, Nijjer S, et al. Baseline Instantaneous Wave-Free Ratio as a Pressure-Only Estimation of Underlying Coronary Flow Reserve. *Circulation: Cardiovascular Interventions* 2014; 7(4): 492–502. doi: 10.1161/circinterventions.113.000926
31. Petraco R, Al-Lamee R, Gotberg M, et al. Real-time use of instantaneous wave-free ratio: Results of the ADVISE in practice: An international, multicenter evaluation of instantaneous wave-free ratio in clinical practice. *American Heart Journal* 2014; 168(5): 739–748. doi: 10.1016/j.ahj.2014.06.022
32. Pisters R, Ilhan M, Veenstra LF, et al. Instantaneous wave-free ratio and fractional flow reserve in clinical practice. *Netherlands Heart Journal* 2018; 26(7-8): 385–392. doi: 10.1007/s12471-018-1125-1
33. Veer vM, Pijls NH, Hennigan B, et al. Comparison of Different Diastolic Resting Indexes to iFR. *Journal of the American College of Cardiology* 2017; 70(25): 3088–3096. doi: 10.1016/j.jacc.2017.10.066
34. Åtberg M, Christiansen EH, Gudmundsdottir IJ, et al. Instantaneous Wave-free Ratio versus Fractional Flow Reserve to Guide PCI. *New England Journal of Medicine* 2017; 376(19): 1813–1823. doi: 10.1056/nejmoa1616540
35. Lee JM, Shin ES, Nam CW, et al. Clinical Outcomes According to Fractional Flow Reserve or Instantaneous Wave-Free Ratio in Deferred Lesions. *JACC: Cardiovascular Interventions* 2017; 10(24): 2502–2510. doi: 10.1016/j.jcin.2017.07.019
36. Maini R, Moscona J, Katigbak P, et al. Instantaneous wave-free ratio as an alternative to fractional flow reserve in assessment of moderate coronary stenoses: A meta-analysis of diagnostic accuracy studies. *Cardiovascular Revascularization Medicine* 2018; 19(5): 613–620. doi: 10.1016/j.carrev.2017.12.014
37. Verardi R, Fioravanti F, Barbero U, et al. Network meta-analysis comparing iFR versus FFR versus coronary angiography to drive coronary revascularization. *Journal of Interventional Cardiology* 2018; 31(6): 725–730. doi: 10.1111/joic.12551
38. Färle T, Bojara W, Meyer S, Elsässer A. Comparison of instantaneous wave-free ratio (iFR) and fractional flow reserve (FFR) — First real world experience. *International Journal of Cardiology* 2015; 199: 1–7. doi: 10.1016/j.ijcard.2015.07.003
39. Cook CM, Jeremias A, Petraco R, et al. Fractional Flow Reserve/Instantaneous Wave-Free Ratio Discordance in Angiographically Intermediate Coronary Stenoses. *JACC: Cardiovascular Interventions* 2017; 10(24): 2514–2524. doi: 10.1016/j.jcin.2017.09.021
40. Iwero F, Cuesta J, Bastante T, et al. Diagnostic accuracy of a hybrid approach of instantaneous wave-free ratio and fractional flow reserve using high-dose intracoronary adenosine to characterize intermediate coronary lesions: Results of the PALS (Practical Assessment of Lesion Severity) pros. *Catheterization and Cardiovascular Interventions* 2017; 90(7): 1070–1076. doi: 10.1002/ccd.27038

41. Davies JE, Sen S, Dehbi HM, et al. Use of the Instantaneous Wave-free Ratio or Fractional Flow Reserve in PCI. *New England Journal of Medicine* 2017; 376(19): 1824–1834. doi: 10.1056/nejmoa1700445
42. Escaned J, Echavarría-Pinto M, Garcia-Garcia HM, et al. Prospective Assessment of the Diagnostic Accuracy of Instantaneous Wave-Free Ratio to Assess Coronary Stenosis Relevance. *JACC: Cardiovascular Interventions* 2015; 8(6): 824–833. doi: 10.1016/j.jcin.2015.01.029
43. Koo B, Erglis A, Doh J, et al. Diagnosis of ischemia-causing coronary stenoses by noninvasive fractional flow reserve computed from coronary computed tomographic angiograms. Results from the prospective multicenter DISCOVER-FLOW (diagnosis of ischemia-causing stenoses obtained Via noninvasive fractional flow reserve) study. *J. Am. Coll. Cardiol.* 2011; 58: 1989–1997. doi: 10.1016/j.jacc.2011.06.066
44. Min J, Leipsic J, Pencina M, et al. Diagnostic accuracy of fractional flow reserve from anatomic CT angiography. *JAMA* 2012; 308: 1237–1245. doi: 10.1001/2012.jama.11274
45. Norgaard B, Leipsic J, Gaur S, et al. Diagnostic performance of noninvasive fractional flow reserve derived from coronary computed tomography angiography in suspected coronary artery disease: the NXT trial (Analysis of Coronary Blood Flow Using CT Angiography: Next Steps). *J. Am. Coll. Cardiol.* 2014; 63: 1145–1155. doi: 10.1016/j.jacc.2013.11.043
46. Morris P, Ryan D, Morton A, et al. Virtual fractional flow reserve from coronary angiography: modeling the significance of coronary lesions: results from the VIRTU-1 (VIRTUal Fractional Flow Reserve From Coronary Angiography) study. *JACC Cardiovasc. Interv.* 2013; 6: 149–157. doi: 10.1016/j.jcin.2012.08.024
47. Papafaklis M, Muramatsu T, Ishibashi Y, et al. Fast virtual functional assessment of intermediate coronary lesions using routine angiographic data and blood flow simulation in humans: comparison with pressure wire fractional flow reserve. *EuroIntervention* 2014; 10: 574–583. doi: 10.4244/EIJY14M07_01
48. Lu S, Barbato E, Kööszegi Z, et al. Fractional flow reserve calculation from 3-dimensional quantitative coronary angiography and TIMI frame count: a fast computer model to quantify the functional significance of moderately obstructed coronary arteries. *JACC Cardiovasc. Interv.* 2014; 7: 768–777. doi: 10.1016/j.jcin.2014.03.004
49. Zhang JM, Zhong L, Luo T, et al. Simplified Models of Non-Invasive Fractional Flow Reserve Based on CT Images. *PLoS ONE* 2016; 11(5): e0153070. doi: 10.1371/journal.pone.0153070
50. Shi C, Zhang D, Cao K, et al. A study of noninvasive fractional flow reserve derived from a simplified method based on coronary computed tomography angiography in suspected coronary artery disease. *Biomed. Eng. Online* 2017; 16: 43. doi: 10.1186/s12938-017-0330-2
51. Renker M, Schoepf U, R. W, et al. Comparison of diagnostic value of a novel noninvasive coronary computed tomography angiography method versus standard coronary angiography for assessing fractional flow reserve. *Am. J. Cardiol.* 2014; 114: 1303–1308. doi: 10.1016/j.amjcard.2014.07.064
52. Boileau E, Nithiarasu P. One-Dimensional Modelling of the Coronary Circulation. Application to Noninvasive Quantification of Fractional Flow Reserve (FFR). In: Tavares J, Jorge R., eds. *Computational and Experimental Biomedical Sciences: Methods and Applications*. 21 of LN Comput. Vis. Biomech. Springer International. 2015 (pp. 137–155).
53. Boileau E, Pant S, Roobottom C, et al. Estimating the accuracy of a reduced-order model for the calculation of fractional flow reserve (FFR). *International Journal for Numerical Methods in Biomedical Engineering* 2017; 34(1): e2908. doi: 10.1002/cnm.2908
54. Baumann S, Wang R, Schoepf U, et al. Coronary CT angiography-derived fractional flow reserve correlated with invasive fractional flow reserve measurements—initial experience with a novel physician-driven algorithm. *Eur. Radiol.* 25; 2015: 1201–2017. doi: 10.1007/s00330-014-3482-5
55. Coenen A, Lubbers M, Kurata A, et al. Fractional flow reserve computed from noninvasive CT angiography data: diagnostic performance of an on-site clinician-operated computational fluid dynamics algorithm. *Radiology* 2015; 274: 674–683. doi: 10.1148/radiol.14140992

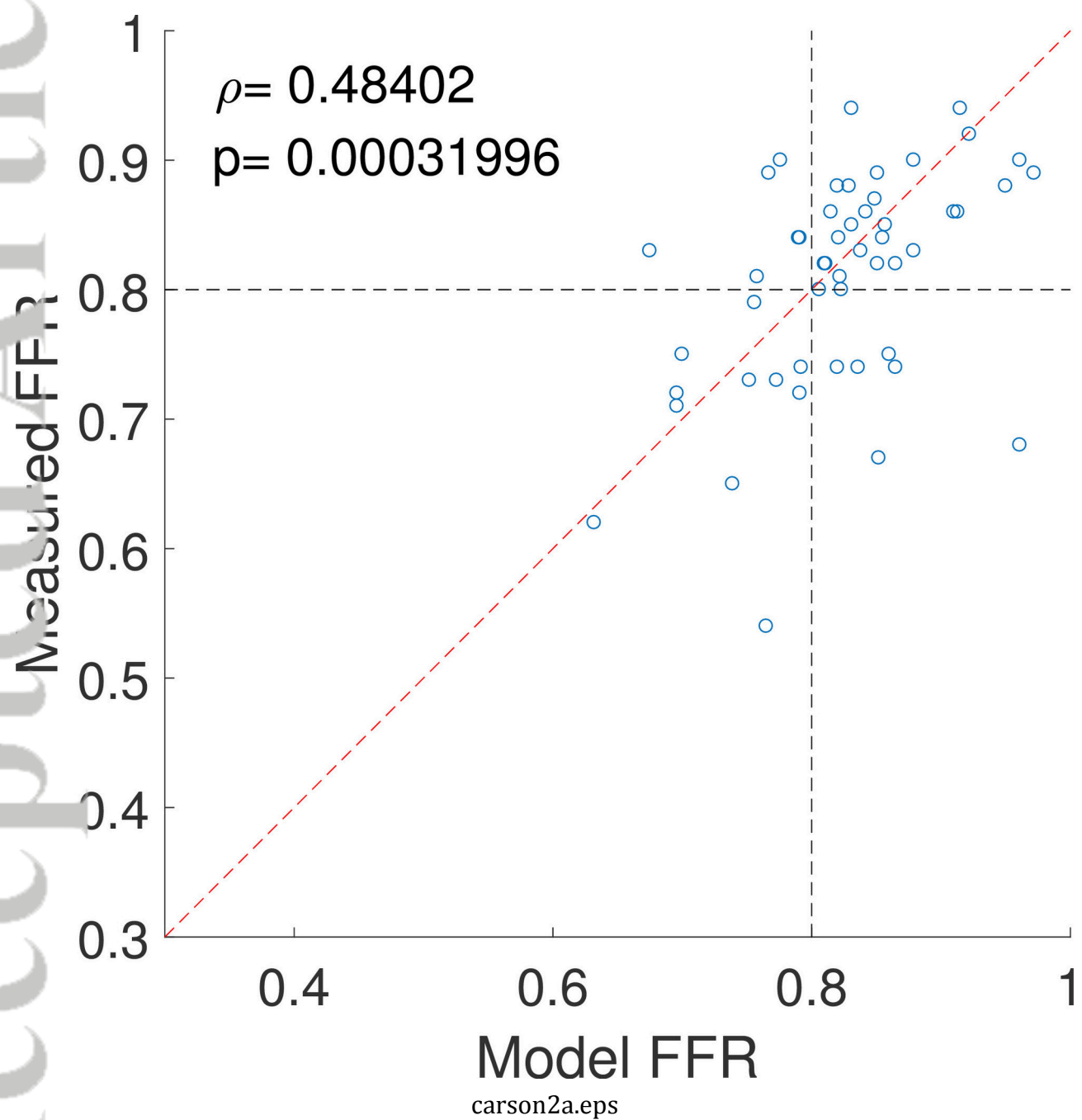
56. Wang R, Renker M, Schoepf U, et al. Diagnostic value of quantitative stenosis predictors with coronary CT angiography compared to invasive fractional flow reserve. *Eur. J. Radiol.* 2015; 84: 1509–1515. doi: 10.1016/j.ejrad.2015.05.010
57. Ma L, Rapaka S, Passerini T, et al. A machine-learning approach for computation of fractional flow reserve from coronary computed tomography. *J. Appl. Physiol.* 2016; 121: 42–52. doi: 10.1152/jappphysiol.00752.2015
58. Röbbs M, Achenbach S, Röther J, et al. Comparison of Fractional Flow Reserve Based on Computational Fluid Dynamics Modeling Using Coronary Angiographic Vessel Morphology Versus Invasively Measured Fractional Flow Reserve. *Am. J. Cardiol.* 2016; 117: 29–35. doi: 10.1016/j.amjcard.2015.10.008
59. Ko B, Cameron J, Munnur R, et al. Noninvasive CT-Derived FFR Based on Structural and Fluid Analysis: A Comparison With Invasive FFR for Detection of Functionally Significant Stenosis. *JACC Cardiovasc. Imaging* 2016. doi: 10.1016/j.jcmg.2016.07.005
60. Blanco PJ, Bulant CA, Müller LO, et al. Comparison of 1D and 3D Models for the Estimation of Fractional Flow Reserve. *Scientific Reports* 2018; 8(1). doi: 10.1038/s41598-018-35344-0
61. Ma Y, Liu H, Hou Y, et al. Instantaneous wave-free ratio derived from coronary computed tomography angiography in evaluation of ischemia-causing coronary stenosis. *Medicine* 2017; 96(4): e5979. doi: 10.1097/md.0000000000005979
62. Wong ASC, Javadzadegan A, Fearon WF, et al. The relationship between coronary artery distensibility and fractional flow reserve. *PLOS ONE* 2017; 12(7): e0181824. doi: 10.1371/journal.pone.0181824
63. Ma L, Passerini T, Badila E, et al. IMAGE-BASED COMPUTATION OF INSTANTANEOUS WAVE-FREE RATIO FROM ROUTINE CORONARY ANGIOGRAPHY: EVALUATION OF A HYBRID DECISION MAKING STRATEGY WITH FFR. *Journal of the American College of Cardiology* 2016; 67(13): 328. doi: 10.1016/s0735-1097(16)30329-1
64. Johnson NP, Kirkeeide RL, Asress KN, et al. Does the Instantaneous Wave-Free Ratio Approximate the Fractional Flow Reserve?. *Journal of the American College of Cardiology* 2013; 61(13): 1428–1435. doi: 10.1016/j.jacc.2012.09.064
65. Calmac L, Niculescu R, Badila E, et al. TCT-40 Image-Based Computation of Instantaneous Wave-free Ratio from Routine Coronary Angiography - Initial Validation by Invasively Measured Coronary Pressures. *Journal of the American College of Cardiology* 2015; 66(15): B17–B18. doi: 10.1016/j.jacc.2015.08.087
66. Carson J. *Development of a cardiovascular and lymphatic network model during human pregnancy*. PhD thesis. 2018.
67. Bessems D, Rutten M, Vosse v. dF. A wave propagation model of blood flow in large vessels using an approximate velocity profile function. *Journal of Fluid Mechanics* 2007; 580: 145-168. doi: 10.1017/S0022112007005344
68. Smith N, Pullan A, Hunter P. An anatomically based model of transient coronary blood flow in the heart. *SIAM J. Appl. Math.* 2002; 62: 990–1018.
69. Mynard JP, Smolich JJ. One-Dimensional Haemodynamic Modeling and Wave Dynamics in the Entire Adult Circulation. *Annals of Biomedical Engineering* 2015; 43(6): 1443–1460. doi: 10.1007/s10439-015-1313-8
70. Olufsen M. Structured tree outflow condition for blood flow in larger systemic arteries. *Am. J. Physiol.* 1999; 276: H257–H268.
71. Carson J, Loon RV. An implicit solver for 1D arterial network models. *International Journal for Numerical Methods in Biomedical Engineering* 2016; 33(7): e2837. doi: 10.1002/cnm.2837
72. Carson J, Lewis M, Rassi D, Loon RV. A data-driven model to study utero-ovarian blood flow physiology during pregnancy. *Biomechanics and Modeling in Mechanobiology* 2019. doi: 10.1007/s10237-019-01135-3
73. Bruyne dB, Bartunek J, Sys SU, Pijls NH, Heyndrickx GR, Wijns W. Simultaneous Coronary Pressure and Flow Velocity Measurements in Humans. *Circulation* 1996; 94(8): 1842–1849. doi: 10.1161/01.cir.94.8.1842
74. Giessen v. dAG, Groen HC, Doriot PA, et al. The influence of boundary conditions on wall shear stress distribution in patients specific coronary trees. *Journal of Biomechanics* 2011; 44(6): 1089–1095. doi: 10.1016/j.jbiomech.2011.01.036

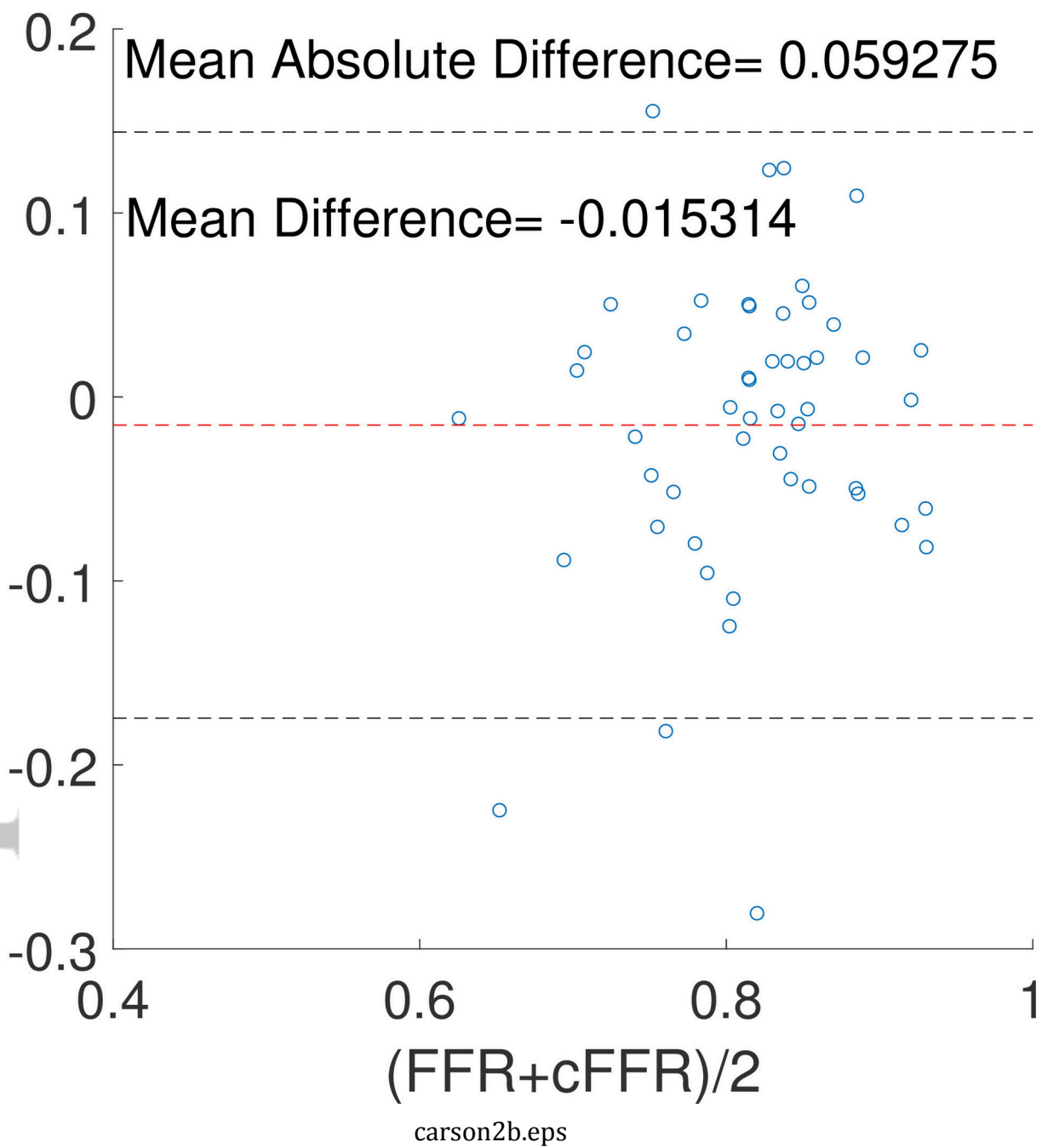
75. Budoff M, Nakanshi R. Noninvasive FFR derived from coronary CT angiography in the management of coronary artery disease: technology and clinical update. *Vascular Health and Risk Management* 2016; 269. doi: 10.2147/vhrm.s79632
76. Todolfi C, Mongiardo A, Spaccarotella C, et al. The instantaneous wave-free ratio (iFR) for evaluation of non-culprit lesions in patients with acute coronary syndrome and multivessel disease. *International Journal of Cardiology* 2015; 178: 46–54. doi: 10.1016/j.ijcard.2014.03.210
77. Kobayashi Y, Johnson NP, Berry C, et al. The Influence of Lesion Location on the Diagnostic Accuracy of Adenosine-Free Coronary Pressure Wire Measurements. *JACC: Cardiovascular Interventions* 2016; 9(23): 2390–2399. doi: 10.1016/j.jcin.2016.08.041
78. Hennigan B, Oldroyd KG, Berry C, et al. Discordance Between Resting and Hyperemic Indices of Coronary Stenosis Severity. *Circulation: Cardiovascular Interventions* 2016; 9(11). doi: 10.1161/circinterventions.116.004016
79. Bede A, Zivelonghi C, Benfari G, et al. iFR-FFR comparison in daily practice. *Journal of Cardiovascular Medicine* 2015; 16(9): 625–631. doi: 10.2459/jcm.0000000000000272
80. Kanaji Y, Murai T, Lee T, et al. Efficacy of pressure parameters obtained during contrast medium-induced submaximal hyperemia in the functional assessment of intermediate coronary stenosis. *International Journal of Cardiology* 2016; 202: 207–213. doi: 10.1016/j.ijcard.2015.09.003
81. Meimoun P, Clerc J, Ardourel D, et al. Assessment of left anterior descending artery stenosis of intermediate severity by fractional flow reserve, instantaneous wave-free ratio, and non-invasive coronary flow reserve. *The International Journal of Cardiovascular Imaging* 2016; 33(7): 999–1007. doi: 10.1007/s10554-016-1000-3
82. Berry C, Veer v. tM, Witt N, et al. VERIFY (VERification of Instantaneous Wave-Free Ratio and Fractional Flow Reserve for the Assessment of Coronary Artery Stenosis Severity in EverydaY Practice). *Journal of the American College of Cardiology* 2013; 61(13): 1421–1427. doi: 10.1016/j.jacc.2012.09.065
83. Takanaka F, Shishido K, Ochiai T, et al. Instantaneous Wave-Free Ratio for the Assessment of Intermediate Coronary Artery Stenosis in Patients With Severe Aortic Valve Stenosis. *JACC: Cardiovascular Interventions* 2018; 11(20): 2032–2040. doi: 10.1016/j.jcin.2018.07.027
84. Mitchell JR. Is the heart a pressure or flow generator? Possible implications and suggestions for cardiovascular pedagogy. *Advances in Physiology Education* 2015; 39(3): 242–247. doi: 10.1152/advan.00057.2015
85. Davies JE, Whinnett ZI, Francis DP, et al. Evidence of a Dominant Backward-Propagating “Suction” Wave Responsible for Diastolic Coronary Filling in Humans, Attenuated in Left Ventricular Hypertrophy. *Circulation* 2006; 113(14): 1768–1778. doi: 10.1161/circulationaha.105.603050
86. Bracco N, Lumley M, Perera D. Fractional flow reserve: conundrums, controversies and challenges. *Interventional Cardiology* 2015; 7(6): 543–552. doi: 10.2217/ica.15.43
87. Boef v. dTP, Nolte F, Rolandi MC, et al. Coronary pressure-flow relations as basis for the understanding of coronary physiology. *Journal of Molecular and Cellular Cardiology* 2012; 52(4): 786–793. doi: 10.1016/j.yjmcc.2011.07.025
88. Schelbert HR. Anatomy and physiology of coronary blood flow. *Journal of Nuclear Cardiology* 2010; 17(4): 545–554. doi: 10.1007/s12350-010-9255-x
89. Lupi A, Buffon A, Finocchiaro ML, Conti E, Maseri A, Crea F. Mechanisms of adenosine-induced epicardial coronary artery dilatation. *European Heart Journal* 1997; 18(4): 614–617. doi: 10.1093/oxfordjournals.eurheartj.a015305
90. Ge X, Yin Z, Fan Y, Vassilevski Y, Liang F. A multi-scale model of the coronary circulation applied to investigate transmural myocardial flow. *International Journal for Numerical Methods in Biomedical Engineering* 2018; e3123. doi: 10.1002/cnm.3123

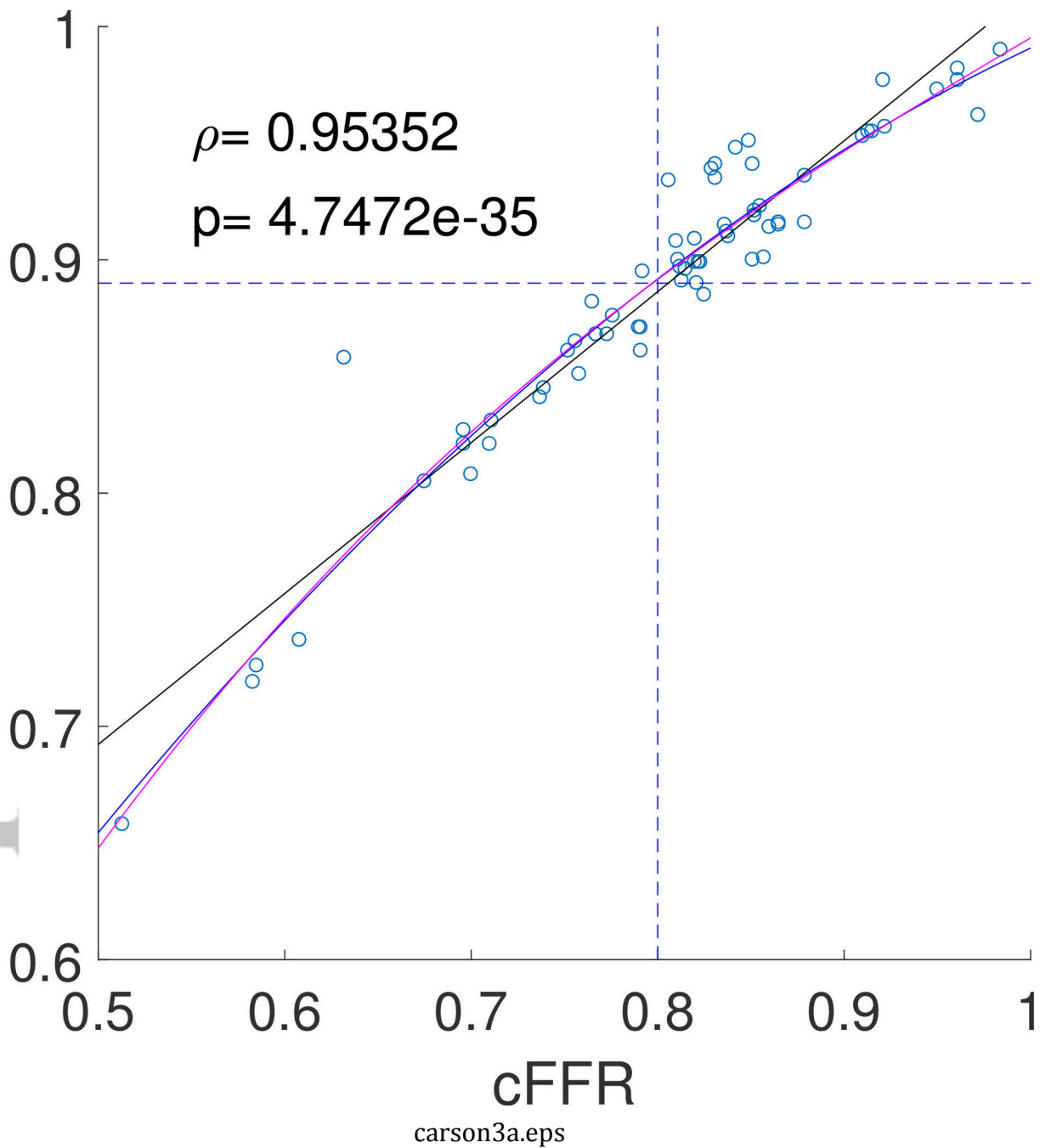


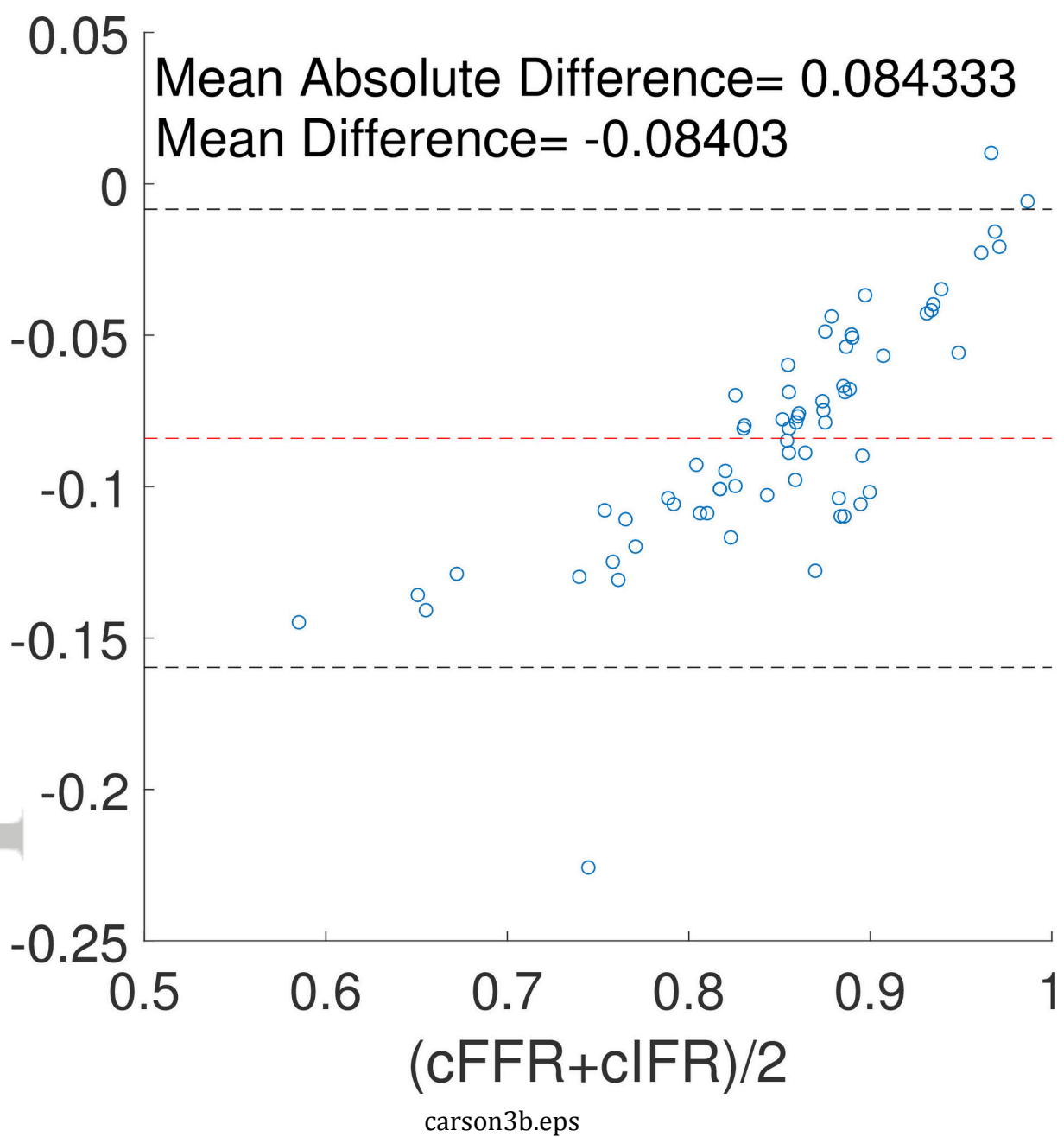


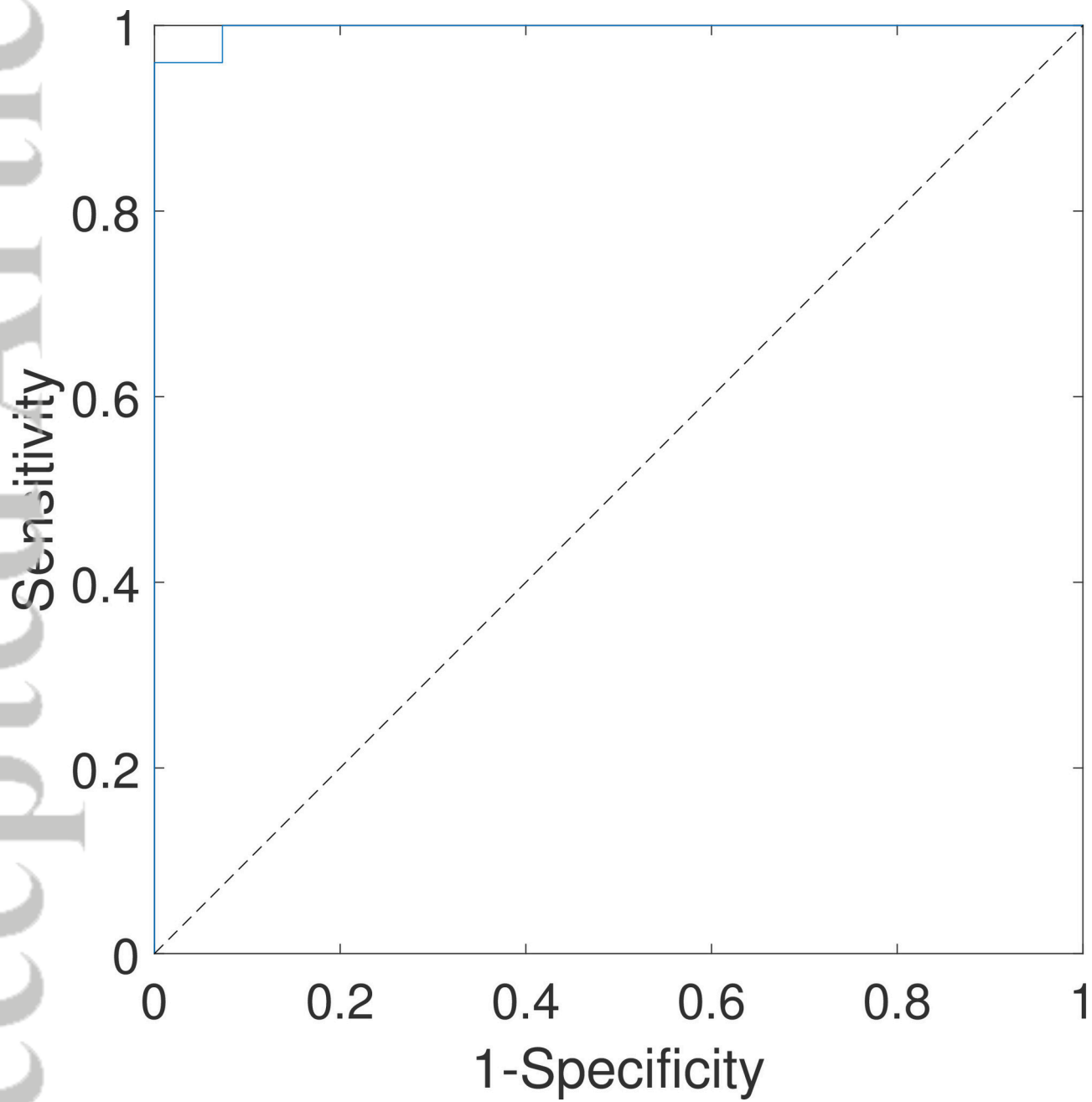
carson1.eps



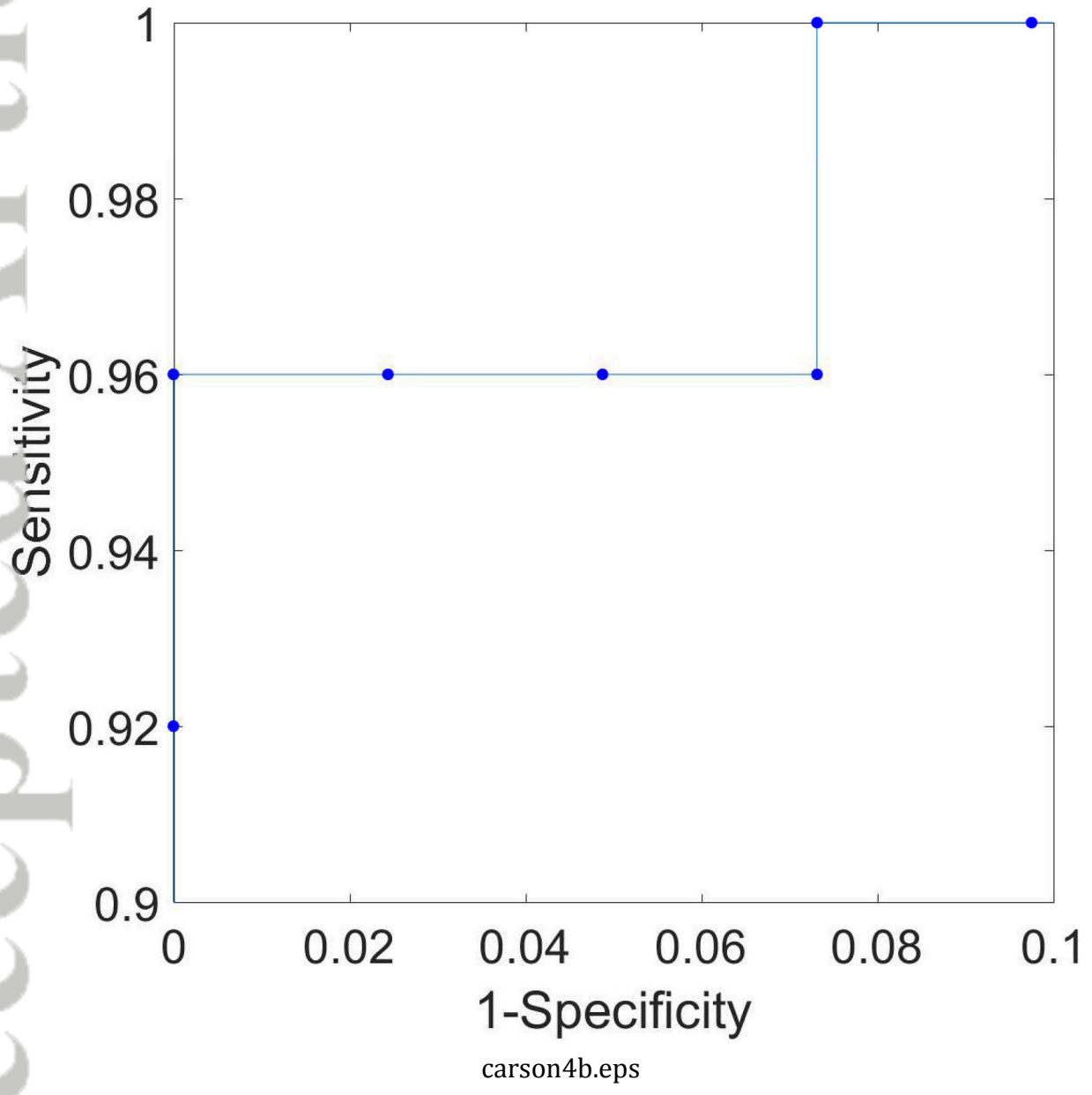


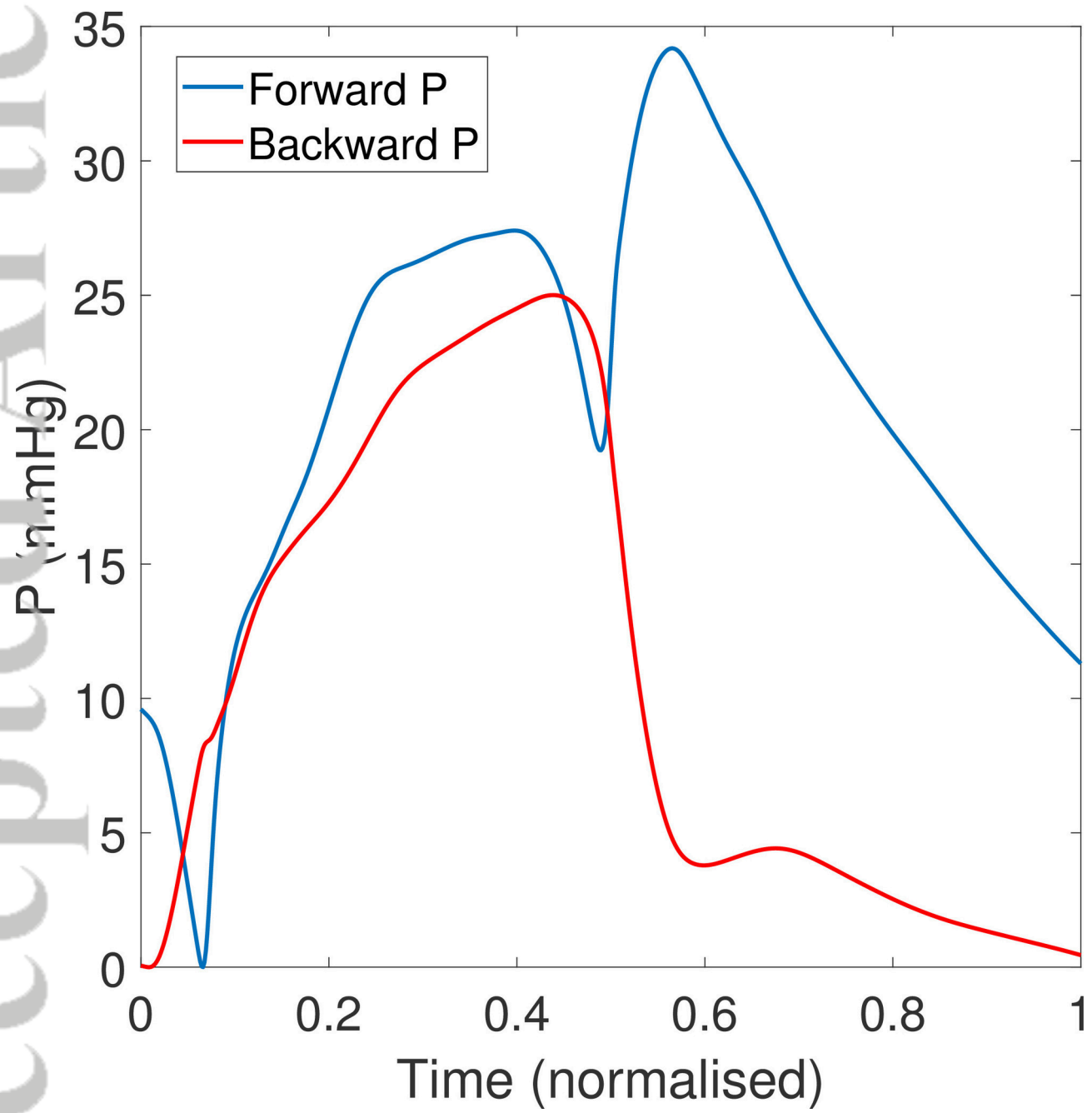




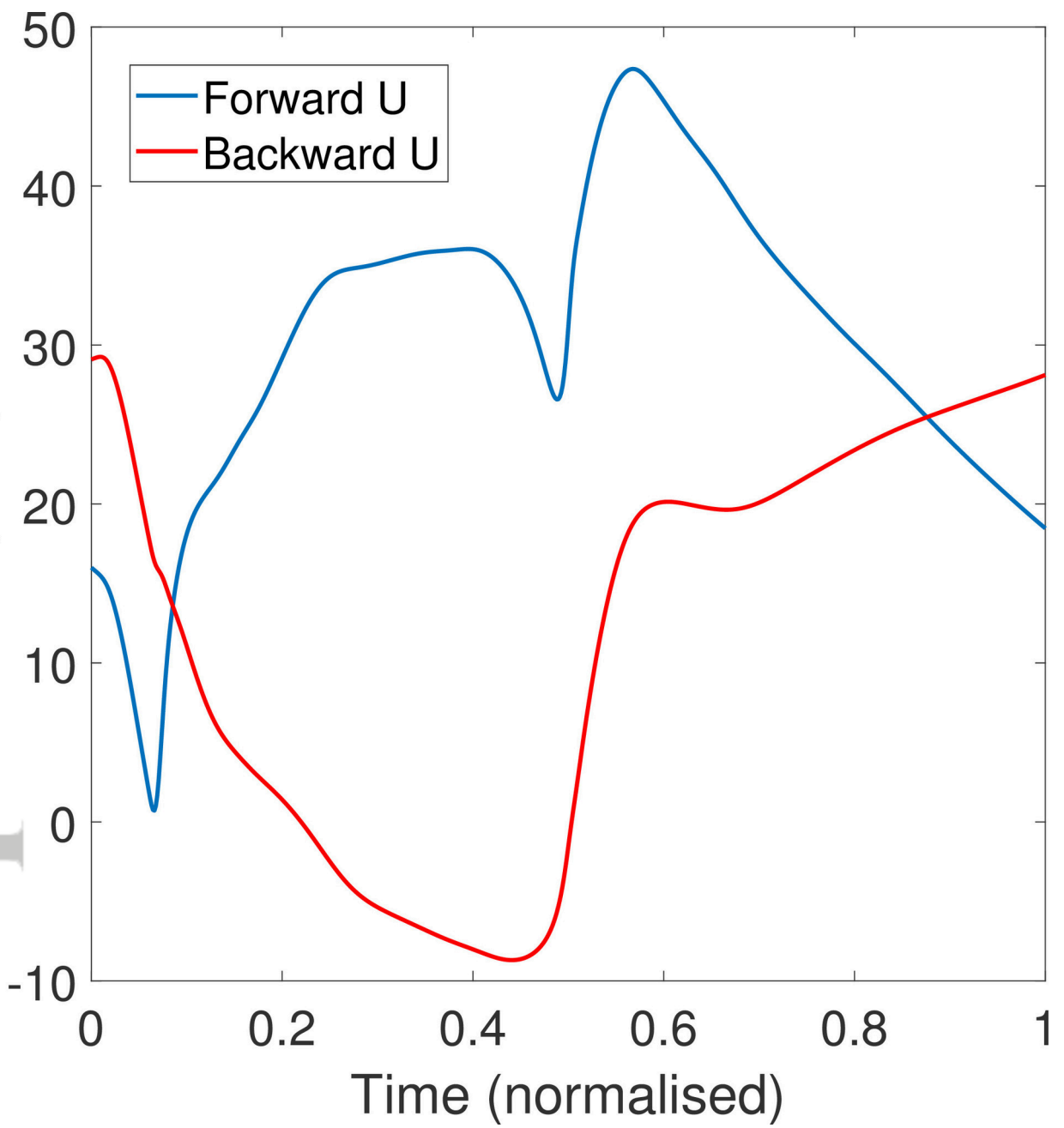


carson4a.eps

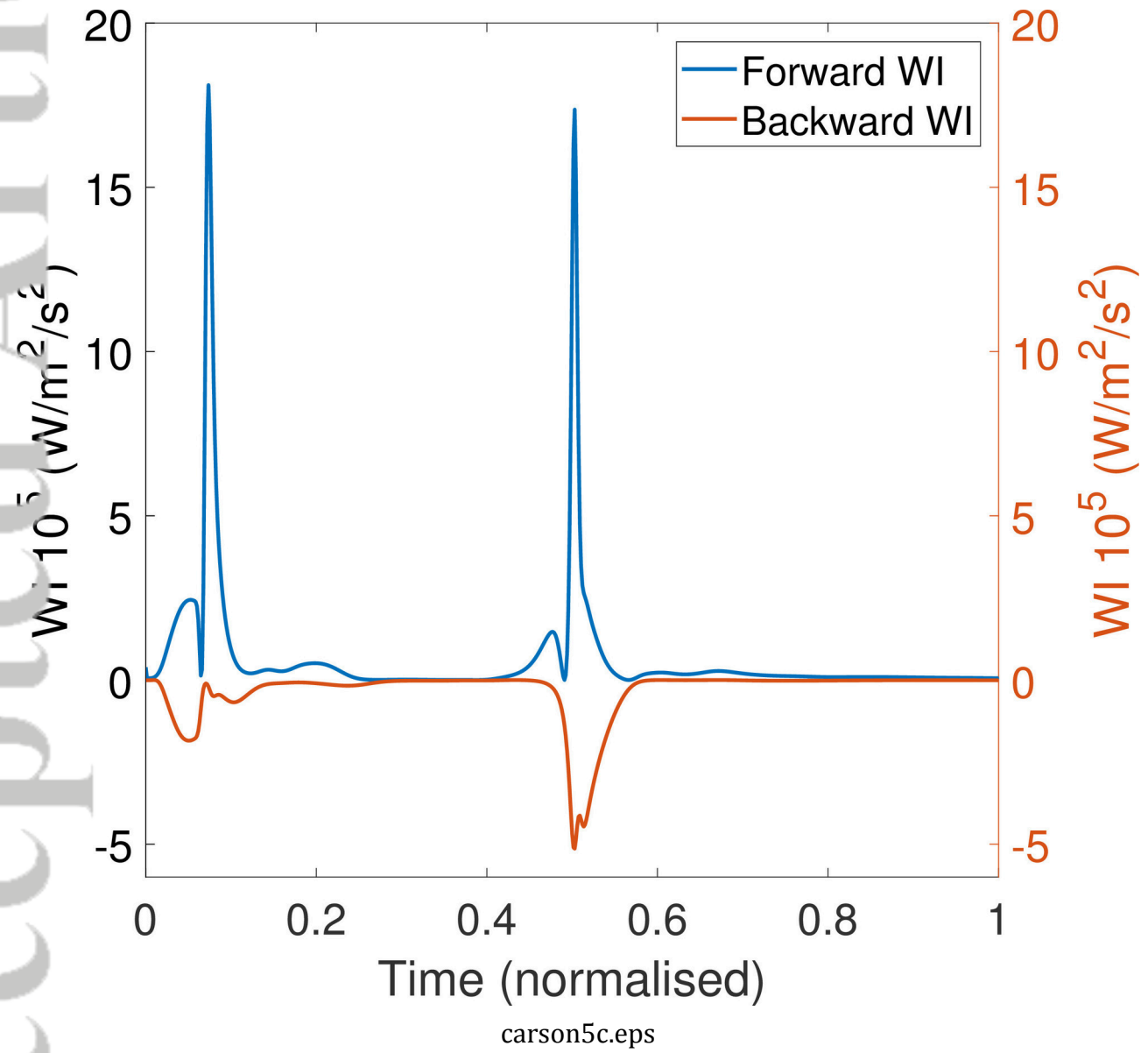




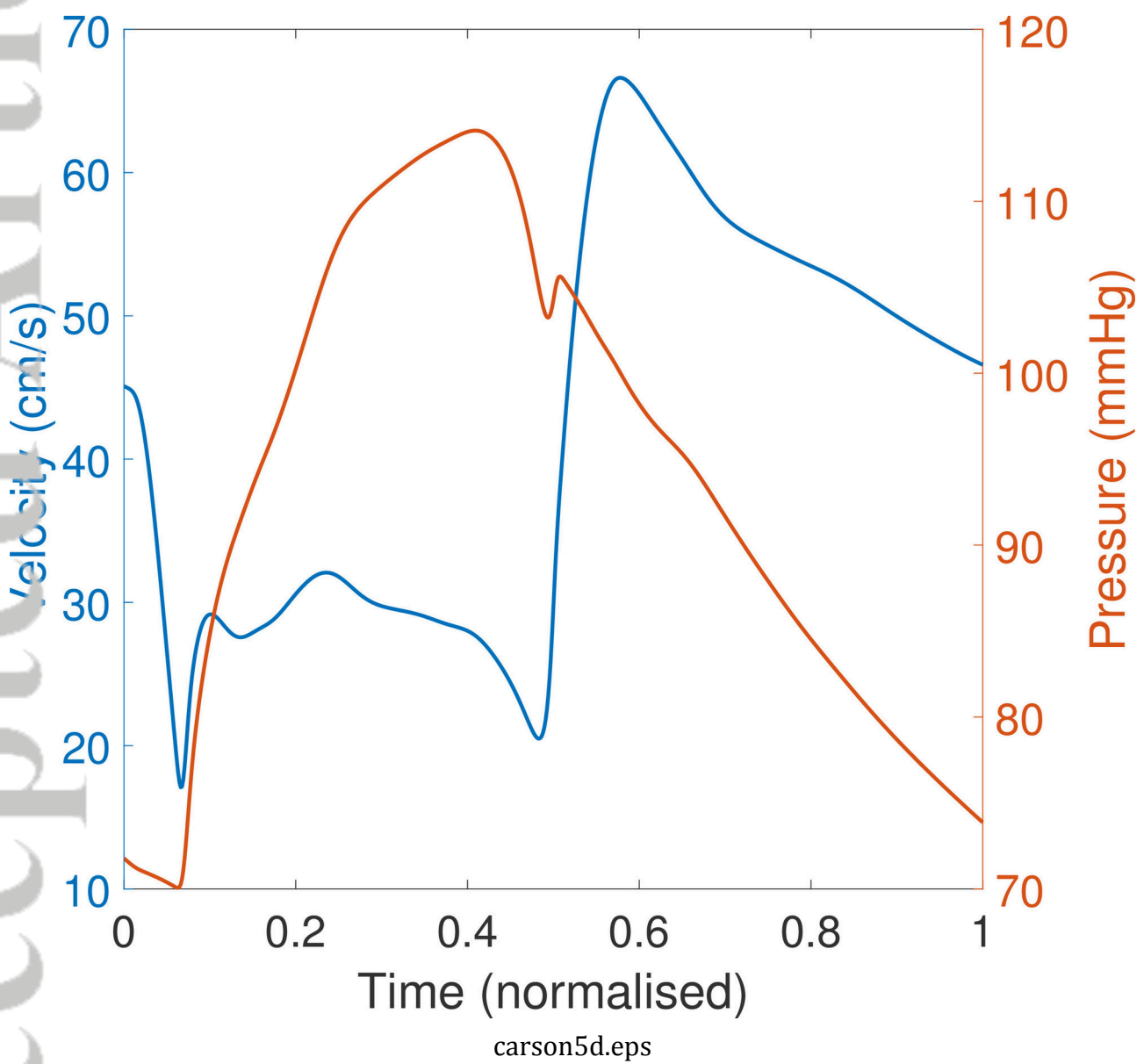
carson5a.eps



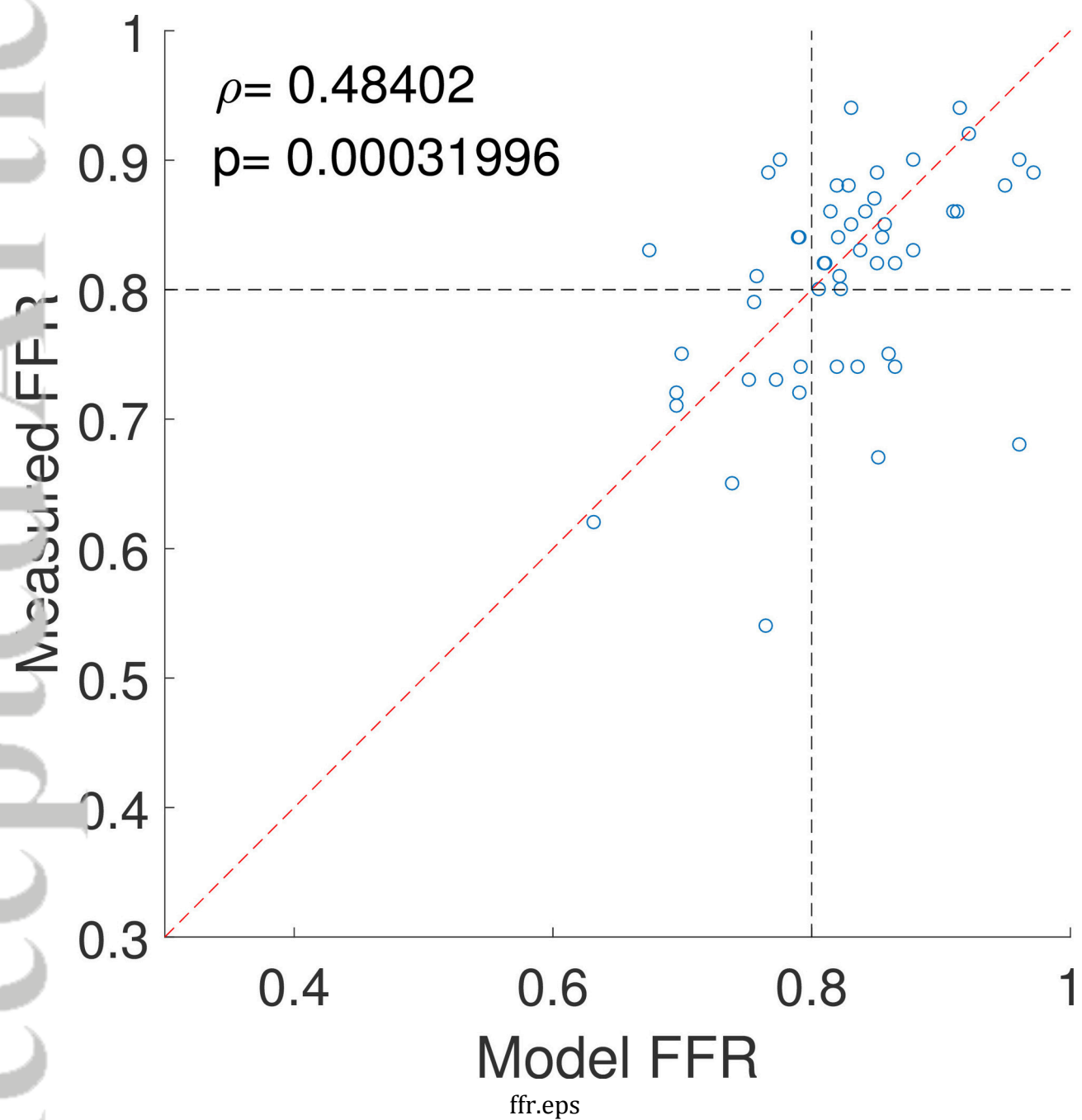
carson5b.eps

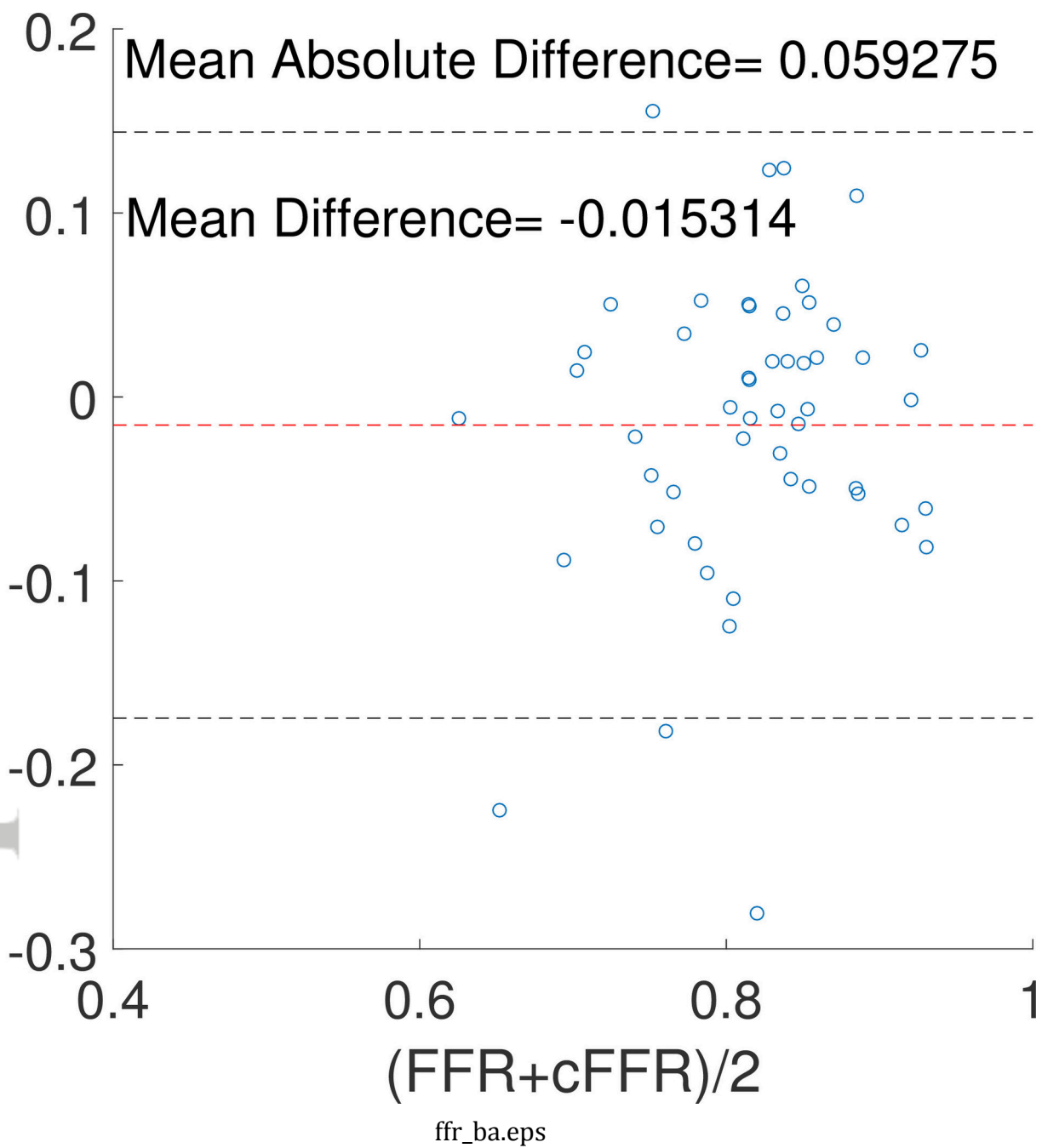


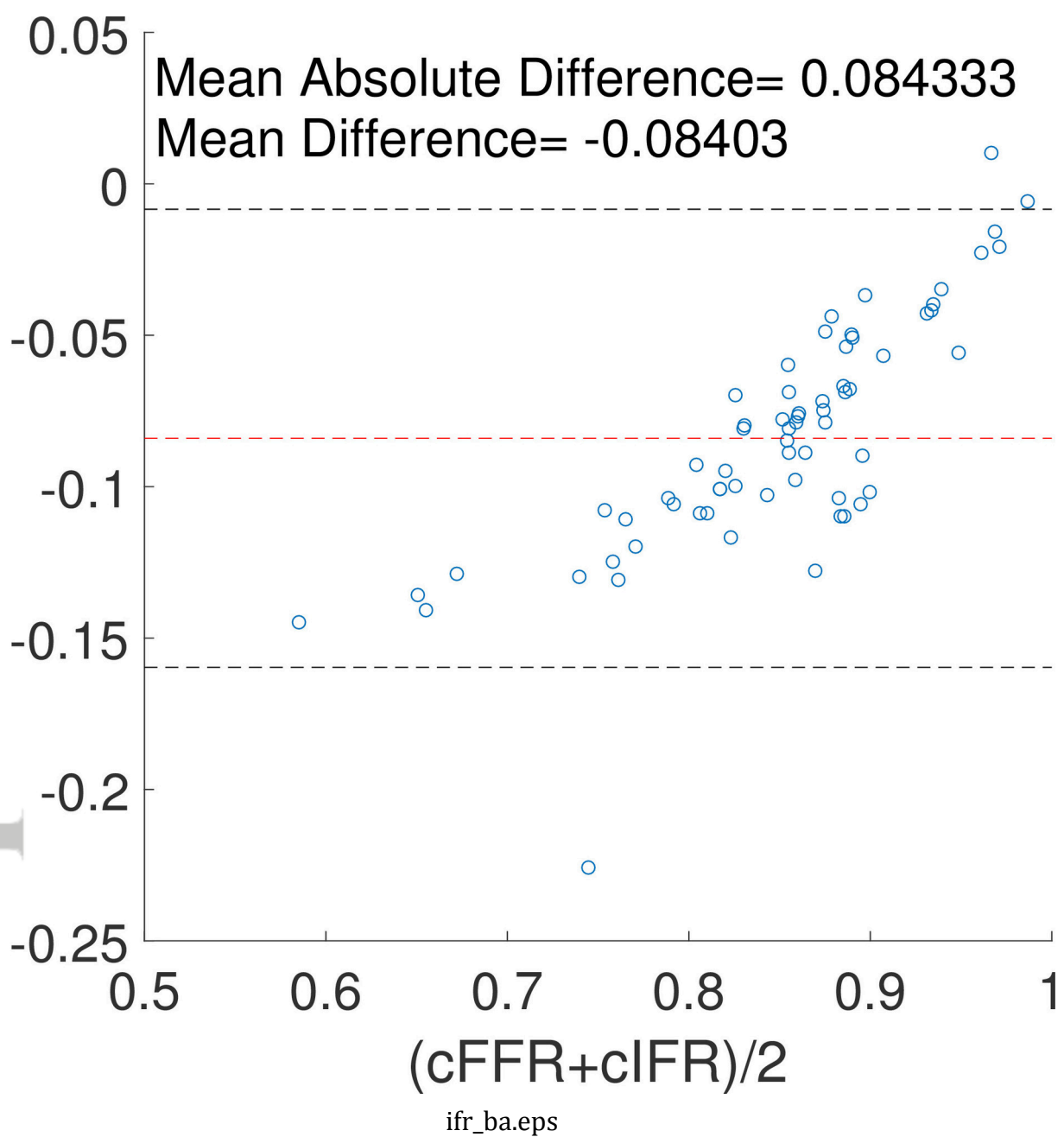
carson5c.eps

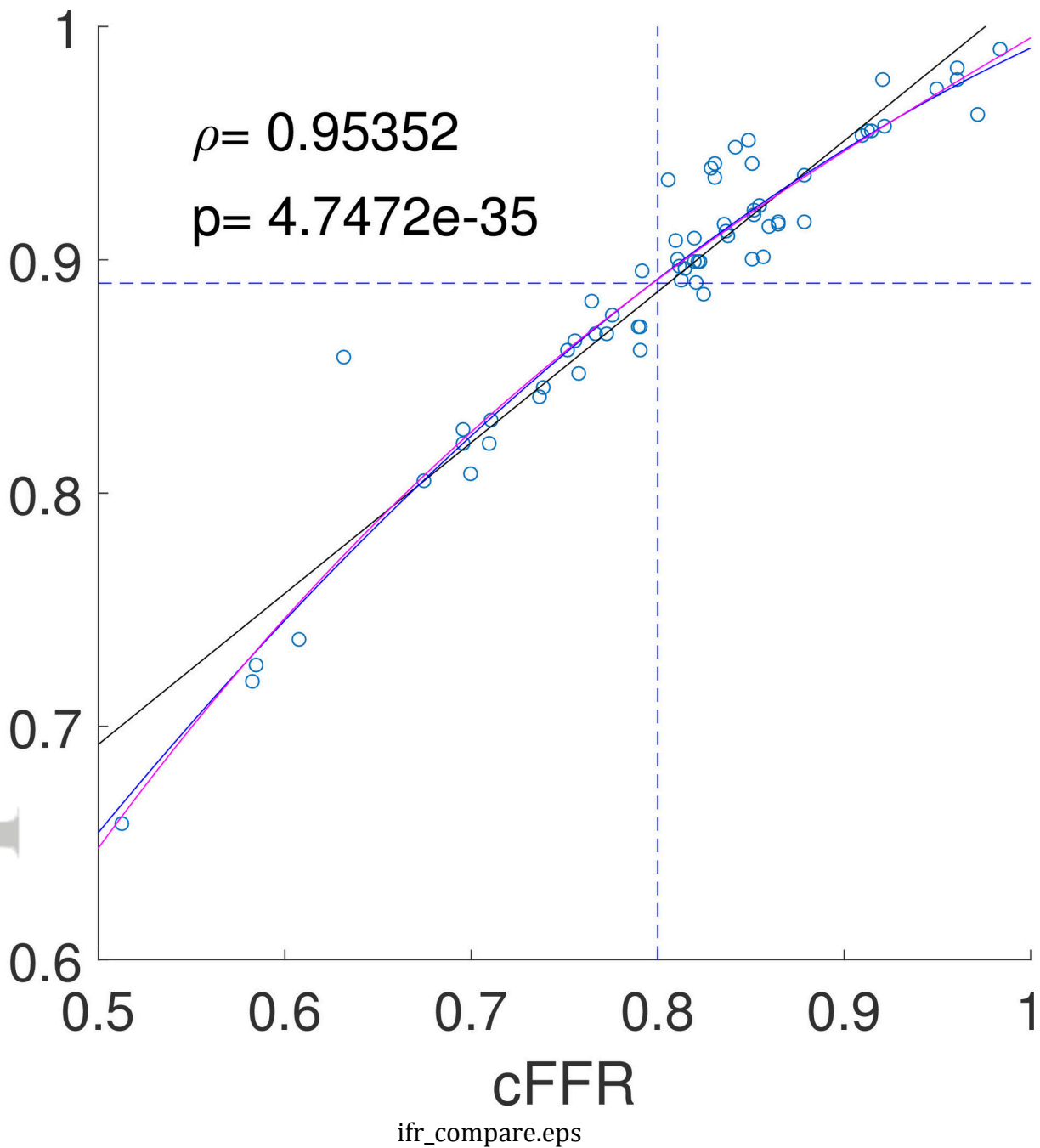


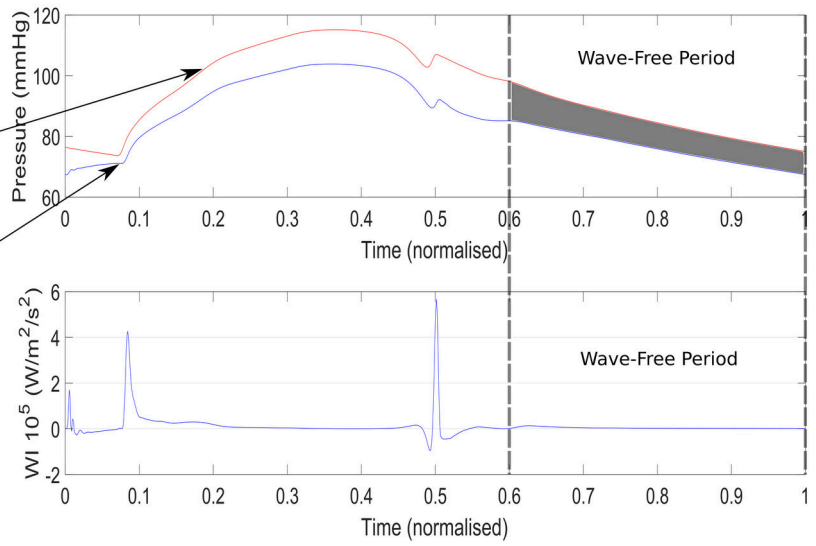
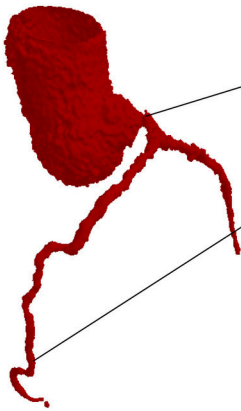
carson5d.eps



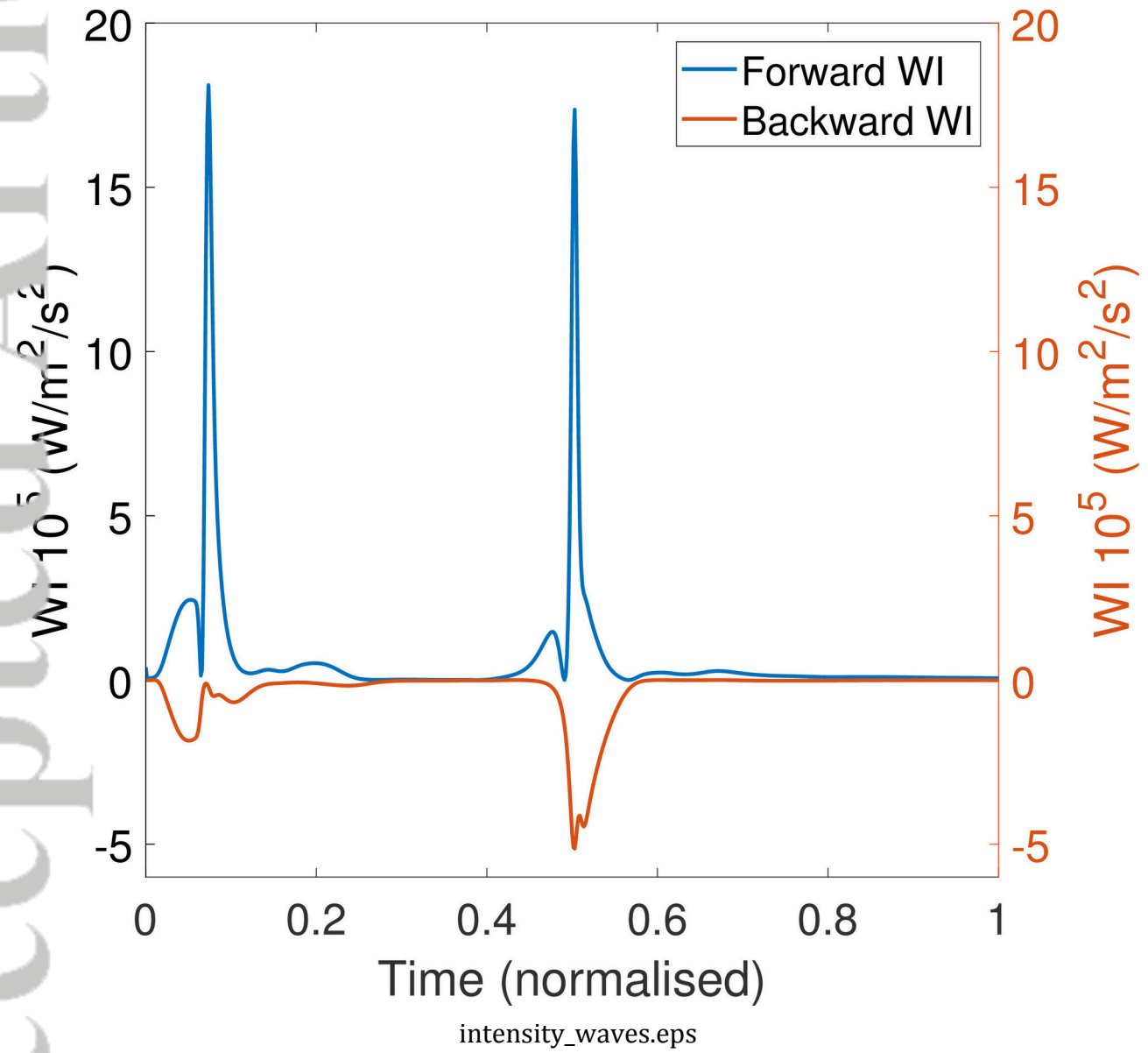


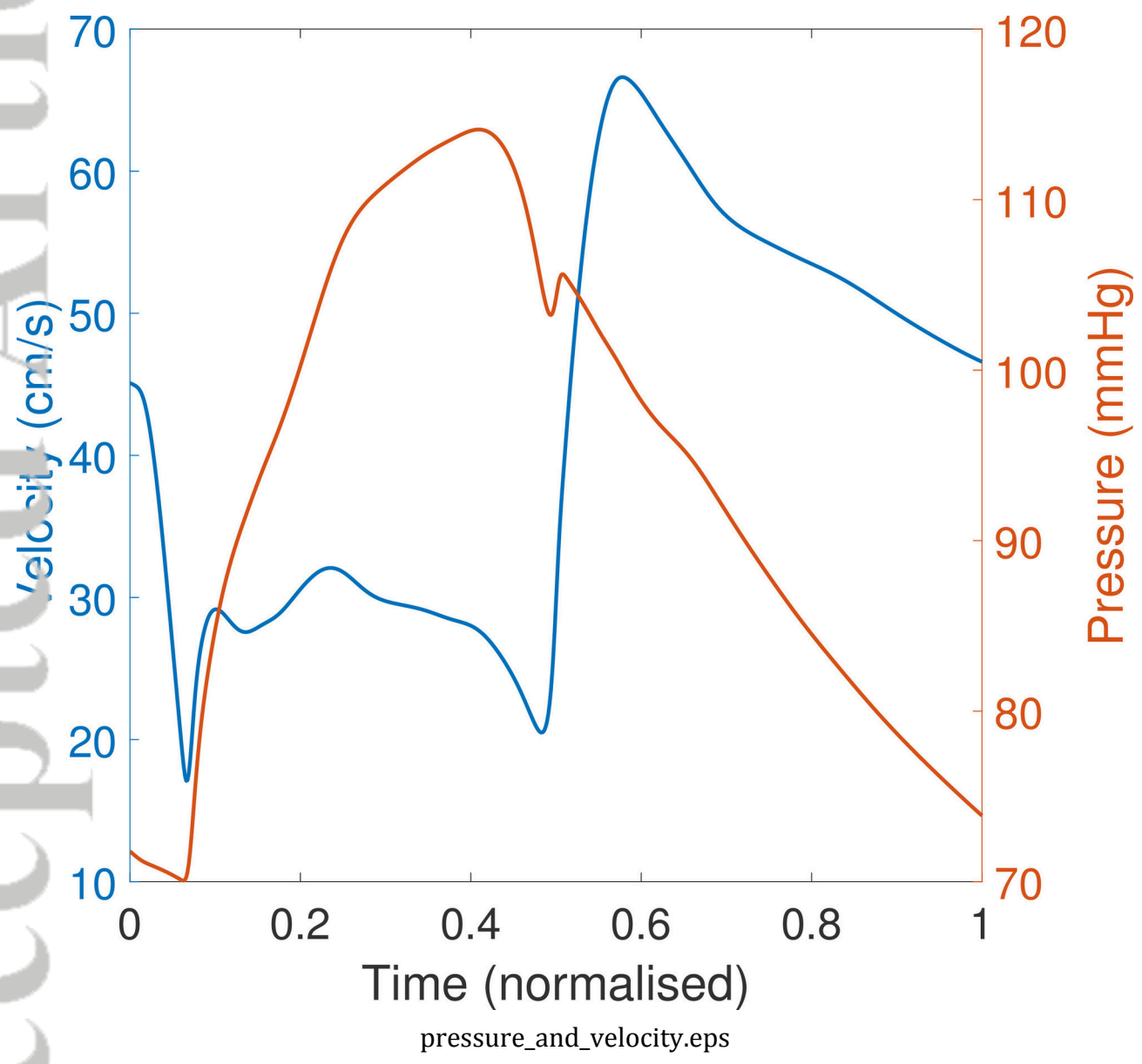


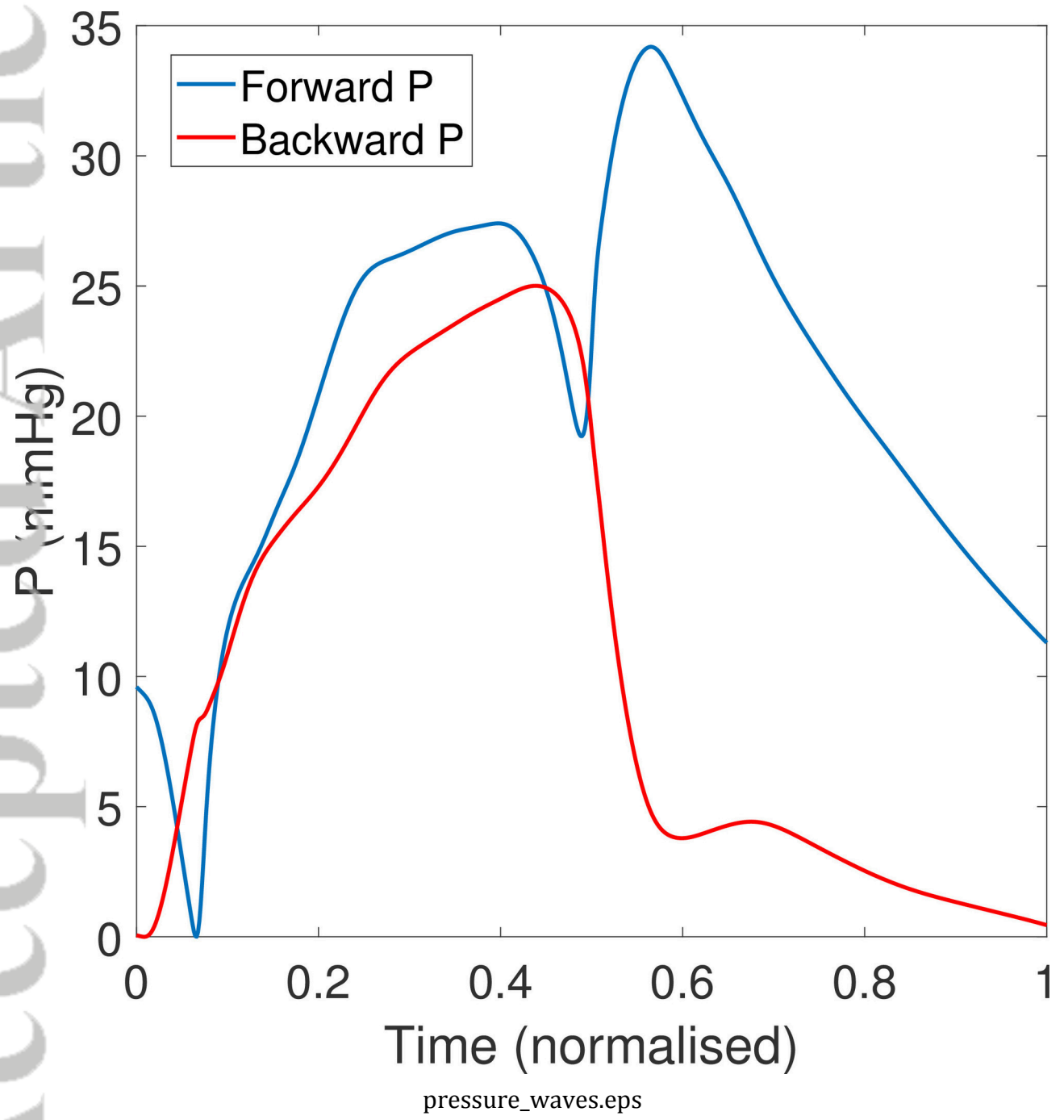


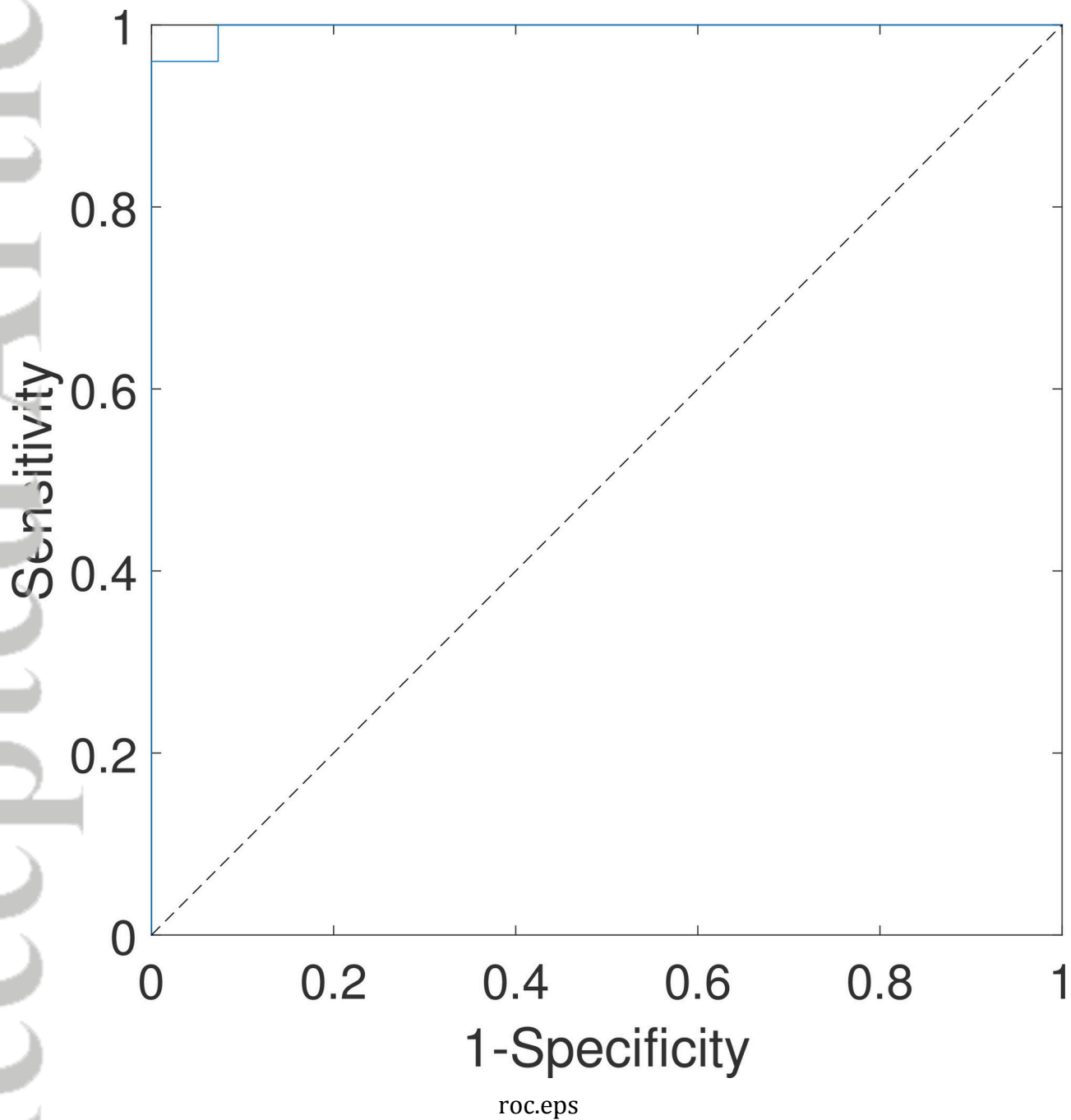


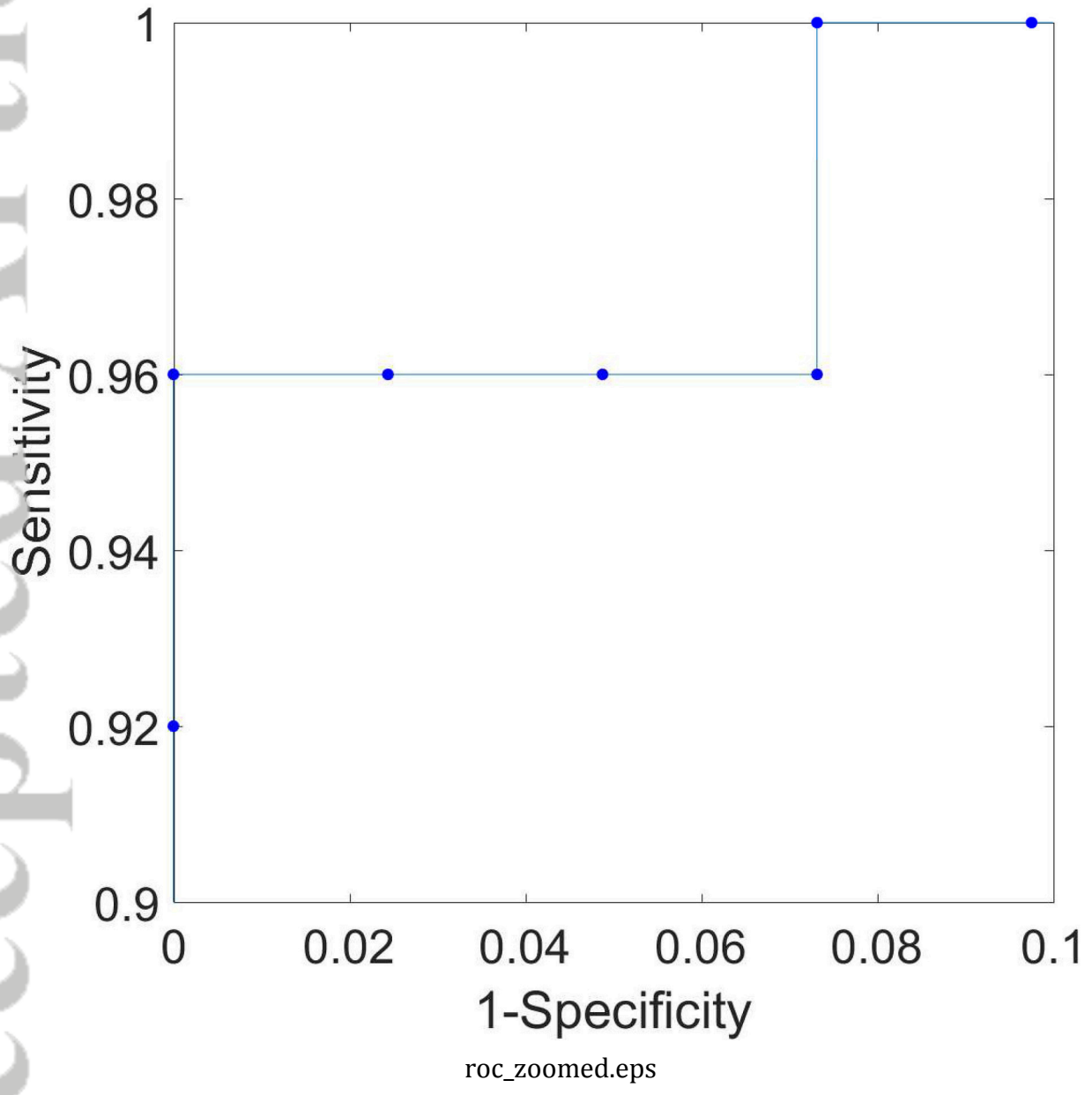
ifr_example.eps

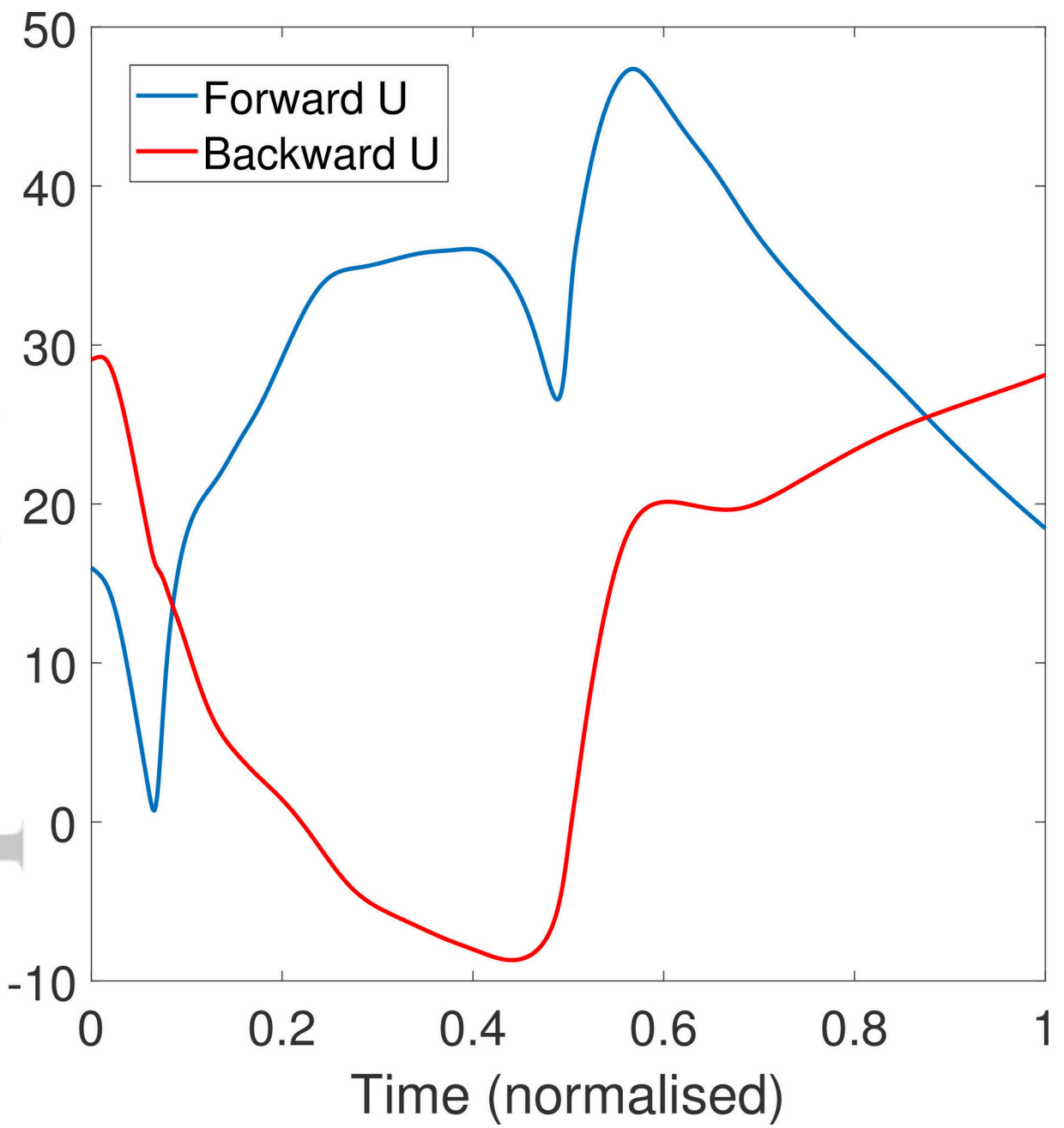












velocity_waves.eps